

Aerodynamic coefficients estimation of a general aviation airplane from flight test data

Haber-Zelanto, David

Master's thesis / Diplomski rad

2021

Degree Grantor / Ustanova koja je dodijelila akademski / stručni stupanj: **University of Zagreb, Faculty of Mechanical Engineering and Naval Architecture / Sveučilište u Zagrebu, Fakultet strojarstva i brodogradnje**

Permanent link / Trajna poveznica: <https://urn.nsk.hr/urn:nbn:hr:235:623552>

Rights / Prava: [In copyright](#)/[Zaštićeno autorskim pravom.](#)

Download date / Datum preuzimanja: **2024-07-15**

Repository / Repozitorij:

[Repository of Faculty of Mechanical Engineering and Naval Architecture University of Zagreb](#)



UNIVERSITY OF ZAGREB
FACULTY OF MECHANICAL ENGINEERING AND NAVAL
ARCHITECTURE

MASTER'S THESIS

David Haber-Zelanto

ZAGREB, 2021.

UNIVERSITY OF ZAGREB
FACULTY OF MECHANICAL ENGINEERING AND NAVAL
ARCHITECTURE

MASTER'S THESIS

AERODYNAMIC COEFFICIENTS ESTIMATION OF A
GENERAL AVIATION AIRPLANE FROM FLIGHT TEST
DATA

Mentors:

Prof. Dr. Sc. Milan Vrdoljak

Dr. Pierluigi Capone

Student:

David Haber-Zelanto

ZAGREB, 2021.

Statement | Izjava

I hereby declare that I have made this thesis independently, given help from my mentors, using the knowledge acquired during my studies and the cited references.

Izjavljujem da sam ovaj rad radio samostalno, uz pomoć mentora, koristeći znanja stečena tijekom studija i navedenu literaturu.

Zagreb, January 2021.

David Haber-Zelanto



SVEUČILIŠTE U ZAGREBU
FAKULTET STROJARSTVA I BRODOGRADNJE
Središnje povjerenstvo za završne i diplomske ispite
Povjerenstvo za završne i diplomske ispite studija zrakoplovstva



Sveučilište u Zagrebu Fakultet strojarstva i brodogradnje	
Datum:	Prilog:
Klasa: 602 - 04 / 21 - 6 / 1	
Ur. broj: 15 - 1703 - 20 -	

DIPLOMSKI ZADATAK

Student: **David Haber Zelanto**

Mat. br.: 0035199010

Naslov rada na
hrvatskom jeziku:

**Estimacija aerodinamičkih koeficijenata za avion opće avijacije iz
podataka s testnih letova**

Naslov rada na
engleskom jeziku:

**Estimation of aerodynamic coefficients of a general aviation airplane
from flight test data**

Opis zadatka:

The Zurich University of Applied Sciences (ZHAW), Centre for Aviation, performed a flight test campaign with the aim to improve the fidelity of ZHAW's existing general aviation airplane Piper PA-28 flight simulator model. The aircraft was instrumented and the flight test campaign in summer 2019 yielded 159 maneuvers that can be used for model development and refinement.

The flight test data recordings, after its processing and organizing, can be used for the estimation of aerodynamic coefficients for the given aircraft. This parameter estimation is highly dependent on the quality and fidelity of the propulsion system model as well as on the model of the aircraft's mass and balance, namely the mass moments of inertia model and center of gravity position.

Following tasks should be performed within the Thesis:

- Processing and organizing of the flight test data in order to prepare data for the parameter estimation;
- Review and improvement of the existing weight and balance model and definition of the model used for parameter estimation;
- Review and improvement of the existing propulsion system model and definition of the model used for parameter estimation;
- Estimation of chosen aerodynamic coefficients using appropriate method, like the simple linear regression model.

Thesis should list used bibliography and any assistance received.

Zadatak zadan:
12. studenoga 2020.

Rok predaje rada:
14. siječnja 2021.

Predviđeni datumi obrane:
18. – 22. siječnja 2021.

Zadatak zadao:

Predsjednik Povjerenstva:

Prof. dr. sc. Milan Vrdoljak

Dr. Pierluigi Capone

Prof. dr. sc. Milan Vrdoljak

Acknowledgement

I would like to thank my co-mentors, prof. Pierluigi Capone and Raphael Monstein for all their support and advice as well as for being good company and providing enjoyable working environment during my stay at ZAV in Winterthur, Switzerland. Big thanks to my mentor prof. Milan Vrdoljak for always being there when needed and for providing me with this opportunity in the first place. Also, I am thankful to Anna Abà for helping me with the part of the work.

Zagreb, January 2021.

David Haber-Zelanto

Contents

Acknowledgement	iv
Contents	v
List of Figures	ix
List of Tables	xii
List of Symbols	xiv
Sažetak	xvii
Summary	xviii
Prošireni sažetak	xix
1. Introduction	1
1.1. Aim and Scope of This Thesis	2
1.2. Structure of the Thesis	3
2. Theoretical Background	4
2.1. Flight Test Data	4
2.1.1. Manoeuvres	4
2.1.2. Instrumentation and Sensors	5
2.1.3. Issues with Flight Test Data	5

2.2. System Identification and Parameter Estimation	7
2.3. Conventions	10
3. Flight Test Data Preparation	11
3.1. Test Aircraft	11
3.1.1. Aircraft Configurations	13
3.2. Data Acquisition	13
3.3. Data Processing	15
3.3.1. Data Collection	16
3.3.2. Delays and Synchronization	17
3.3.3. Calibration	17
3.3.4. Sensor Error Models	18
3.3.5. Calculations	19
3.3.6. Cutting Data to Manoeuvres	19
3.3.7. Data Structure	21
4. Mass, Balance and Inertia	23
4.1. Mass Estimation	23
4.1.1. Mass Distribution and OEM Estimation	23
4.1.2. Actual Mass of the Aircraft	24
4.2. Inertia and CG estimation	26
4.2.1. Main Moments of Inertia	27
4.2.2. Center of Gravity Position	30
4.2.3. Cross Moments of Inertia	30
4.3. Results and Comparison	31
5. Propulsion	33
5.1. Engine Model	33
5.2. Throttle Mapping	35
5.2.1. Engine Model Initialization	37
5.3. Engine Forces and Moments	38
6. Data Corrections	39
6.1. Data Correction for IMU Installation Angle	39

6.2. Filtering FTD Parameters	43
6.3. Off-CG Corrections	46
6.4. Correcting Air Data	47
6.4.1. Air Data Boom	47
6.4.2. Flight Path Reconstruction	48
6.4.3. Correcting Air Data for off-CG Position	52
7. Aerodynamic Coefficients	55
8. Parameter Estimation With Linear Regression	58
8.1. Introduction to modelling	59
8.2. Base models	60
8.3. Longitudinal motion coefficients	60
8.3.1. Pitching moment coefficient model	60
8.3.2. Lift force coefficient model	63
8.3.3. Drag force coefficient model	65
8.4. Lateral motion	67
9. Conclusions	71
Bibliography	73
A. Appendix A	75
A.1. Flight Test Data Processing	75
A.1.1. Flight Test Data	75
A.1.2. Data Processing Utilities	75
A.1.3. Processed Data	76
B. Appendix B	77
B.1. Mass, Balance and Inertia Estimation	77
B.2. Propulsion	77
B.3. Flight Test Data Assembly and Corrections	77
B.4. Modelling and Regression	78
B.5. Flight Path Reconstruction	78

C. Appendix C	79
C.1. Measurements	79
C.1.1. IMU position	79
C.1.2. ADB position	81

List of Figures

0.1	ReDSim simulator na Centru za zrakoplovstvo na Sveučilištu primjenjenih znanosti u Zürichu	xx
0.2	Testni zrakoplov HB-PRL, Piper Pa-28-161 Warrior III	xxi
0.3	Pregled obrade podataka	xxii
0.4	Usporedba izmjerenih okretaja po minuti i okretaja motora izračunatih modelom	xxiv
0.5	Izmjerena i filtrirana linearna ubrzanja za jedan kratkotrajni manevar . .	xxvi
0.6	Korekcije podataka za poziciju težišta za jedan kratkotrajni manevar i jedan <i>dutch-roll</i> manevar	xxvii
0.7	Linearna regresija koeficijenta momenta propinjanja za niz kratkotrajnih manevara	xxviii
0.8	Linearna regresija koeficijenta sile uzgona za niz fugoidnih manevara . . .	xxix
0.9	Regresija koeficijenta sile otpora za niz manevara sloma uzgona	xxix
1.1	Test aircraft Piper Pa-28-161	1
1.2	ReDSim simulator at ZHAW	2
2.1	System identification scheme	7
2.2	Definition of system identification, parameter estimation and simulation .	8
2.3	”Quad-M” methodology	9
2.4	axis definition	10
3.1	Test aircraft HB-PRL, Piper Pa-28-161 Warrior III	11
3.2	Top, front and side view of the test aircraft	12

3.3	Ekinox 2, IMU from manufacturer SBG Systems	14
3.4	IMU and cRIO with it's 7 C-modules mounted in baggage compartment .	15
3.5	Data processing overview	16
3.6	True airspeed <i>TAS</i> for a stall, phugoid, dutch roll and steady heading steady sideslip manoeuvre	20
4.1	Station reference lines from AMM	26
4.2	Aircraft coordinate system	27
4.3	Front view of the basic reconstructed CAD model	28
4.4	Left side view of the basic reconstructed CAD model	28
4.5	Top view of the basic reconstructed CAD model	28
5.1	Standalone PA-28 Simulink engine model	34
5.2	RPM of the older version of the engine model RPM compared to the measured RPM	35
5.3	Mapping process of the power setting	36
5.4	Engine model RPM with throttle mapping compared to the measured RPM	36
5.5	Closer view of the engine model transient behaviour	37
5.6	Final engine model response with initialisation of the engine implemented	38
6.1	Measuring the water line level of the aircraft	40
6.2	Baggage floor (IMU installation angle) angle with reference to the air- craft's water line	40
6.3	Correction of rotational rates and linear accelerations for misalignment angle $\alpha_{IMU} = 4.75^\circ$ for a short period manoeuvre	42
6.4	Measured and filtered rotational rates p, q, r for a short period manoeuvre	44
6.5	Measured and filtered linear accelerations a_x, a_y, a_z for a short period manoeuvre	45
6.6	Air Data Boom (ADB) measurement unit	48
6.7	FPR results for a phugoid, three stall manoeuvres and a steady heading steady sideslip manoeuvre	49
6.8	FPR results for three short period manoeuvres and 2 dutch rolls	50
6.9	Sensor error model corrections to air data for one short period manoeuvre and one stall manoeuvre	52

6.10	Off-CG air data correction for a short period and a dutch roll manoeuvre	54
8.1	C_m regression with a base model	61
8.2	C_m regression with improved model, for a span of short period manoeuvres	62
8.3	C_m regression with improved model, for a span of stall manoeuvres . . .	62
8.4	C_L model regression for a span of stall manoeuvres	64
8.5	C_L model regression for a span of phugoid manoeuvres	64
8.6	C_D model regression for a span of stall manoeuvres	66
8.7	C_D model regression for a span of phugoid manoeuvres	66
8.8	C_Y model regression for a span of steady heading steady sideslip manoeuvres	68
8.9	C_n model regression for a span of dutch roll and bank-to-bank manoeuvres	69
C.1	Measuring IMU z position	80
C.2	Measuring ADB x position	81

List of Tables

0.1	Pozicije težišta za maksimalnu težinu bez goriva (OEM) te za maksimalnu težinu pri polijetanju (ATOM)	xxiii
0.2	Maseni momenti tromosti za maksimalnu težinu bez goriva (OEM) te za maksimalnu težinu pri polijetanju (ATOM)	xxiii
0.3	Primjer sila i momenata motora za mali vremenski interval kratkotrajnog manevra	xxv
0.4	Procijenjeni parametri modela koeficijenta momenta propinjanja	xxviii
2.1	Control surface deflections convention	10
3.1	General dimensions of the PA-28	12
3.2	Some data calibration values taken from	18
3.3	Naming convention of the manoeuvre data files	20
3.4	Final data structure with all the parameters from flight test campaign	21
4.1	Estimates comparison with weighting values	31
4.2	CG position in ACS	32
4.3	Mass moments of inertia estimates in ACS	32
5.1	Example of the engine forces and moments in BCS for an instance of a short period manoeuvre	38
8.1	Estimated parameters for a pitching moment coefficient model	63
8.2	Estimated parameters for the lift force coefficient model	65
8.3	Estimated parameters for the drag force coefficient model	67

8.4	Estimated parameters for the side force coefficient model	68
8.5	Estimated parameters for the yaw moment coefficient model	69
8.6	Estimated parameters for the roll moment coefficient model	70

List of Symbols

$[a_x, a_y, a_z]$	Linear acceleration components in body frame, $[\text{m/s}^2]$	22
A2B	Matrix of transformation from ACS to BCS	47
AR	Aspect ratio, [-]	12
b	Wing span, [m]	12
$[C_l, C_m, C_n]$	Aerodynamic moment coefficients, [-]	57
$[C_x, C_y, C_z]$	Aerodynamic force coefficients, [-]	57
c_r	Wing root chord, [m]	12
C_T	Thrust coefficient, [-]	57
c_t	Wing tip chord, [m]	12
D_{RPCG}	CG-RP lever arm vector, [m]	57
F_{aero}	Aerodynamic force vector, [N]	57
F_{eng}	Engine force vector, [N]	57
$I_{0x,0y,0z}$	Mass moments of inertia around section centroid	27
$I_{x,y,z}$	Mass moments of inertia around the remote axes	27
$I_{xx,yy,zz}$	Aircraft's main moments of inertia	27
$[L, M, N]$	Aircraft moments in body frame, [Nm]	10
$[L_e, M_e, N_e]$	Engine moments in body frame, [Nm]	38
L_y	Rotational matrix around the y axis	42
\bar{c}	Mean aerodynamic chord, [m]	12
M_{aero}	Aerodynamic moments vector, [Nm]	57
M_{eng}	Engine moments vector, [Nm]	57
I_C	Local cross moment of inertia around the centroid, $[\text{kgm}^2]$	31

$I_{xy,xz,yz}$	Cross moments of inertia, [kgm ²]	31
M	Mach number, [-]	54
m	Mass, [kg]	30
M_{x,y,z_i}	Section moment around the remote axes, [Nm]	30
$M_{x,y,z_{total}}$	Total moments around the remote axes, [Nm]	30
$[\dot{p}, \dot{q}, \dot{r}]$	Rotational rate components derivatives, [deg/s ²]	47
$[p, q, r]$	Body axes rotational rate components, [deg/s]	22
$[p^*, q^*, r^*]$	Normalized rotational rate components, [-]	47
p_s	Static pressure, [Pa]	19
PA	Pressure altitude, [m]	19
q_c	Dynamic pressure, [Pa]	19
R	Specific molar mass of air, [J kg ⁻¹ K ⁻¹]	19
S_{ref}	Referent wing area, [m ²]	12
T	Temperature, [K]	19
t	Time, [s]	47
TAS	True airspeed, [m/s]	19
$[u, v, w]$	Velocity components in body frame, [m/s]	47
$[x, y, z]$	Coordinates in ACS, [m]	47
$[x_0, y_0, z_0]$	Remote axes offsets from ACS, [m]	30
$[X_e, Y_e, Z_e]$	Engine forces in body frame, [N]	38
α	Angle of attack, [deg]	19
β	Angle of sideslip, [deg]	19
δ	Control surface deflection, [deg]	10
δ_a	Aileron deflection, [deg]	10
δ_e	Elevator deflection, [deg]	10
δ_r	Rudder deflection, [deg]	10
γ	Heat capacity ratio of air, [-]	54
∇	Gradient, [-]	47
Ω	Rotational rates vector, [rad/s]	57
ω_c	Cutt-off frequency, [rad s ⁻¹]	45
$[\phi, \theta, \psi]$	Roll, Pitch and Yaw angle, [deg]	22
ρ	Air density, [kg/m ³]	19

Subscripts

<i>ADB</i>	Denoting the ADB location	47
<i>CG</i>	Denoting the CG location	47
<i>corr</i>	Defining a corrected parameter	47
<i>i</i>	Defining a structural section	47
<i>IMU</i>	Denoting the IMU location	47
<i>m</i>	Measured Parameter	47
<i>RP</i>	Denotes the reference point	57

Abbrevatons

ACS	Aircraft Coordinate System	14
ADB	Air Data Boom	5
AMM	Airplane Maintenance Manual	26
AoA	Angle of Attack	5
AoS	Angle of Sideslip	5
ATOM	Aircraft Take Off Mass	23
BCS	Body Coordinate System	10
CG	Center of gravity	23
DAQ	Data Acquisition	22
FPR	Flight Path Reconstruction	3
FTD	Flight Test Data	5
FTE	Flight Test Engineer	15
GPS	Global Positioning System	5
IMU	Inertial Measurement Unit	5
MEMS	Micro-Electro-Mechanical-Systems	14
OAT	Outside Air Temperature	5
OEM	Operating Empty Mass	23
POH	Pilot's Operating Handbook	13
RPM	Revolutions Per Minute	5
TAT	True Air Temperature	5
USAF	United States Air Force	27
ZAV	Center for Aviation	1
ZHAW	Zurich University of Applied Sciences	1

Sažetak

Na ljetu 2019. godine Centar za zrakoplovstvo na Sveučilištu primijenjenih znanosti u Zürichu proveo je kampanju letnih ispitivanja na avionu Piper Pa-28-161. Od tada im je cilj razvitak samostalnog modela Pipera PA-28 koji se može primijeniti u njihovom istražnom simulatoru. Ovaj se diplomski rad bavi prikupljanjem svih potrebnih podataka i postavljenjem procedure za postupak procjene parametara modela aerodinamičkih koeficijenata. Uz osnovni uvod u identifikaciju sustava i procjenu parametara, u radu je dan i pregled ispitnih podataka iz leta, instrumentacije i ispitnih točaka, zajedno s izazovima i problemima koje treba spomenuti prije nego što se podaci mogu upotrijebiti. Nakon obrade podataka iz leta, prikazano je kako se vrši procjena mase, ravnoteže i inercije zrakoplova. Slijedi proračun sila i momenata motora, potrebnih za izračun aerodinamičkih koeficijenata. Predstavljene su i dodatne korekcije podataka i razvoj modela pogrešaka senzora postupkom rekonstrukcije putanje leta. Konačno, nakon što su svi podaci okupljeni i strukturirani, vrši se procjena parametara linearnom regresijom metodom najmanjih kvadrata. Također su postavljeni i primjermi modeli aerodinamičkih koeficijenata.

Ključne riječi: procjena parametara, Piper PA-28-161, podaci iz leta, model pogrešaka senzora, rekonstrukcija putanje leta, aerodinamički koeficijenti, linearna regresija, momenti tromosti, model motora, manevar.

Summary

In the summer of 2019 the Center for Aviation at the Zürich University of Applied Sciences conducted a flight test campaign on a Piper Pa-28-161 airplane. Since then, they have the goal of a self-made model of a Piper PA-28 which can be implemented in their Research and Didactics Simulator. This thesis is concerned with all the necessary data gathering and set up for a parameter estimation process determining aerodynamic coefficient models. Along with the basic introduction to the system identification and parameter estimation, this thesis provides an overview of the flight test data, instrumentation and test points together with some challenges and issues that have to be mentioned before the data can be used. After the processing procedure of the flight test data, it is shown how the estimation of the mass, balance and inertia of the aircraft is performed. Next, engine forces and moments needed for aerodynamic coefficient calculation are computed. Additional data corrections and sensor error model development with flight path reconstruction is presented as well. Finally, after all the data is gathered and assembled, parameter estimation with linear estimation is done using the ordinary least squares method. Exemplary models of the aerodynamic coefficients are offered as well.

Keywords: parameter estimation, Piper PA-28-161, flight test data, sensor error model, flight path reconstruction, aerodynamic coefficients, linear regression, moments of inertia, engine model, manoeuvre.

Prošireni sažetak

Uvod

Na ljetu 2019. godine Centar za zrakoplovstvo na Sveučilištu primijenjenih znanosti u Zürichu proveo je kampanju letnih ispitivanja na avionu Piper Pa-28-161 koja se sastoji od 159 različitih testnih točaka u 9 testnih letova. Centar za zrakoplovstvo, od tada, ima za cilj razviti samostalnog modela Pipera PA-28 koji se može primijeniti u njihovom istražnom simulatoru. ReDSim simulator (slika 0.1) je osnovan 2011. godine od strane zaposlenika i studenata koji su u to vrijeme pisali svoje diplomske radove. Simulator pruža izvrsnu podlogu za različita istraživanja na području dinamike leta kao i za laboratorijske vježbe. Na istom se mogu simulirati različite vrste letjelica i njihovih konfiguracija.



Slika 0.1: ReDSim simulator na Centru za zrakoplovstvo na Sveučilištu primjenjenih znanosti u Zürichu

Cilj ovog diplomskog rada je prikupljanje, obrada i strukturiranje svih potrebnih podataka iz leta te dodatnih vrijednosti potrebnih za izračun aerodinamičkih koeficijenata. Samim time, namjera rada je i postavljanje cjeloukupnog procesa za procjenu parametara modela aerodinamičkih koeficijenata te razvitak osnovnih modela linearnom regresijom uz pomoć metode najmanjih kvadrata. Svi razvijeni i poboljšani podsustavi bi se naposljetku trebali unijeti u postojeći PA-28 model u simulatoru dovodeći ga na neku novu, višu razinu.

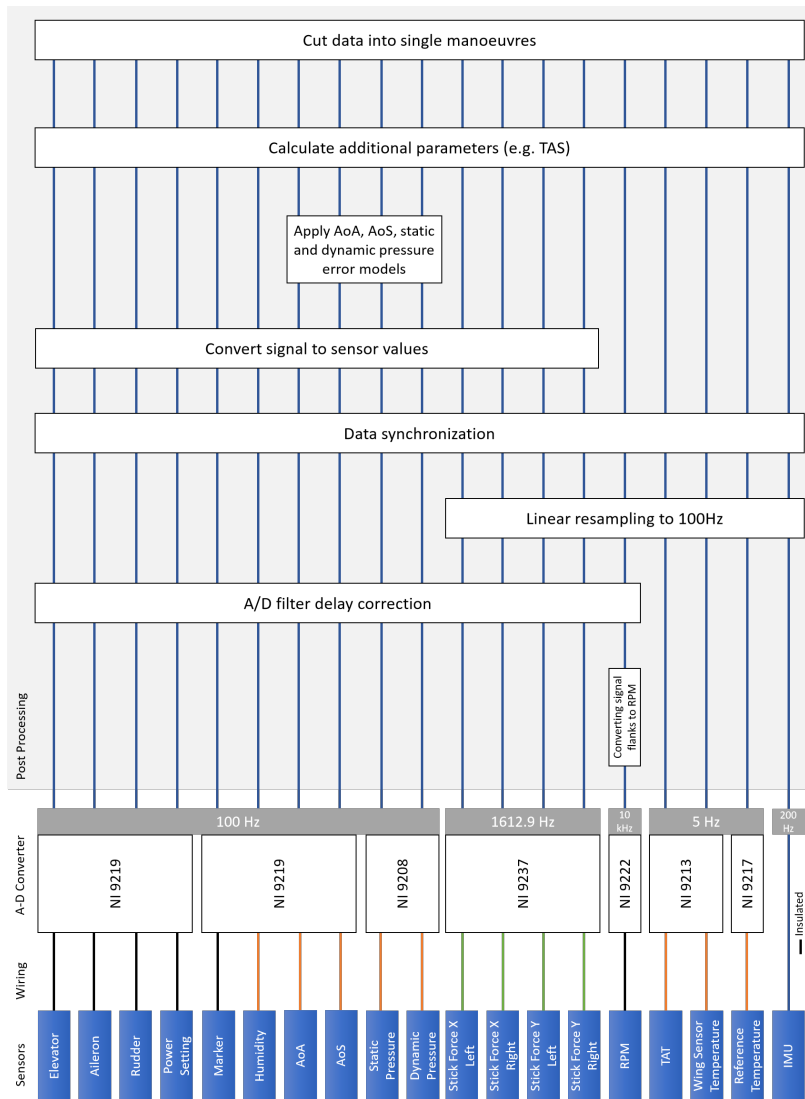
Priprema podataka

Kao što je rečeno, testni zrakoplov bio je Piper Pa-28-161 Warrior III (slika 0.2) koji je, za potrebe testne kampanje, dodatno opremljen mjernim instrumentima. Oni uključuju inercijsku jedinicu, jedinicu za mjerenje zračnih podataka (napadni kut, kut klizanja, statički i dinamički tlak) te razne druge instrumente za mjerenje temperature, količine vlage, parametara motora, zvuka, otklona upravljačkih površina te sila na palicu.



Slika 0.2: Testni zrakoplov HB-PRL, Piper Pa-28-161 Warrior III [1]

Iako su podaci iz leta već obrađeni kroz prijašnja dva diplomatska rada [1] i [2], u sklopu ovog rada su ponovno obrađeni, na dosljedniji način. Podaci su najprije prikupljeni i obrađeni kroz više razina obrade. One uključuju sakupljanje podataka, sinkronizaciju, kalibriranje, korekciju, dodatne kalkulacije, podjelu podataka po manevrima i na kraju strukturiranje. Pregled obrade podataka prikazan je na slici 0.3.



Slika 0.3: Pregled obrade podataka [2]

Masa i inercija

Nakon obrade podataka potrebno je izračunati još neke veličine potrebne za izračun aerodinamičkih koeficijenata. Prvo, potrebne su vrijednosti mase, balansa (pozicije težišta) i masenih momenata tromosti. Promjena mase, kroz različite letove i manevre, te pozicije težišta su dobivene uz pomoć metoda procjene razvijenih u [1]. Iste su unaprijedene u sklopu ovog rada te je dodana procjena poprečnih momenata tromosti. Poboljšana je i procjena mase koja sada uključuje promjenu razine goriva i konfiguracije posade. Pozicije težišta za maksimalnu težinu bez goriva (OEM) te za maksimalnu težinu pri polijetanju (ATOM) prikazane su u tablici 0.1.

Tablica 0.1: Pozicije težišta za maksimalnu težinu bez goriva (OEM) te za maksimalnu težinu pri polijetanju (ATOM)

	OEM [m]	ATOM [m]
x_{CG}	2.2531	2.2509
y_{CG}	0	-0.0032
z_{CG}	-0.07	-0.104

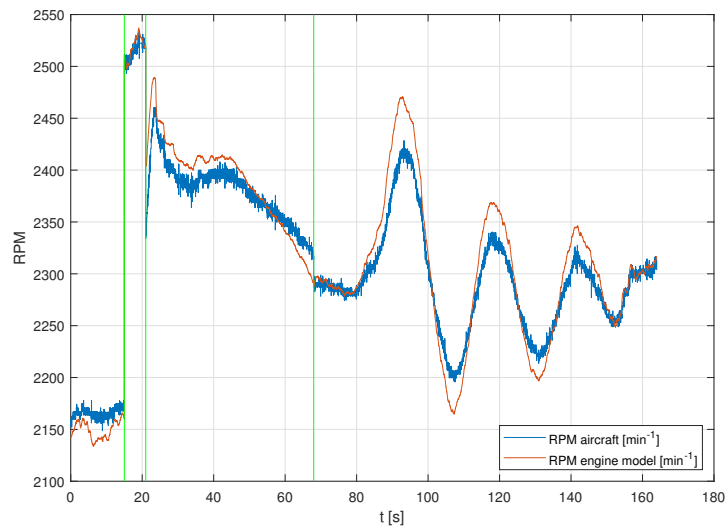
Također, prikazani su (tablica 0.2) i procijenjeni maseni momenti tromosti za dvije prethodno definirane težine.

Tablica 0.2: Maseni momenti tromosti za maksimalnu težinu bez goriva (OEM) te za maksimalnu težinu pri polijetanju (ATOM)

	OEM [kgm ²]	ATOM [kgm ²]
I_{xx}	1513.0	1890.3
I_{yy}	2082.1	2160.9
I_{zz}	3490.8	3861.6
I_{xy}	0	-5.4
I_{xz}	74.17	61.2
I_{yz}	0	2.2

Model motora

Još jedne od potrebnih veličina jesu sile i momenti motora. One su dobivene služeći se postojećim PA-28 Simulink modelom motora. Na početku, model nije pružao rezultate koji su se podudarali sa izmjerenim parametrima motora. Zbog toga je razvijena funkcija koja ulazni parametar ručice gasa prilagođava vrijednostima koje za izlazne paramere daju rezultate odgovarajuće izmjerenima. Na slici 0.4 vide se izmjereni okretaji po minuti (RPM aircraft) u usporedbi sa okretajima izračunatih modelom motora (RPM engine model).



Slika 0.4: Usporedba izmjerenih okretaja po minuti i okretaja motora izračunatih modelom

Sile i momenti motora za jedan mali vremenski period kratkotrajnog manevra prikazani su u tablici 0.3.

Tablica 0.3: Primjer sila i momenata motora za mali vremenski interval kratkotrajnog manevra

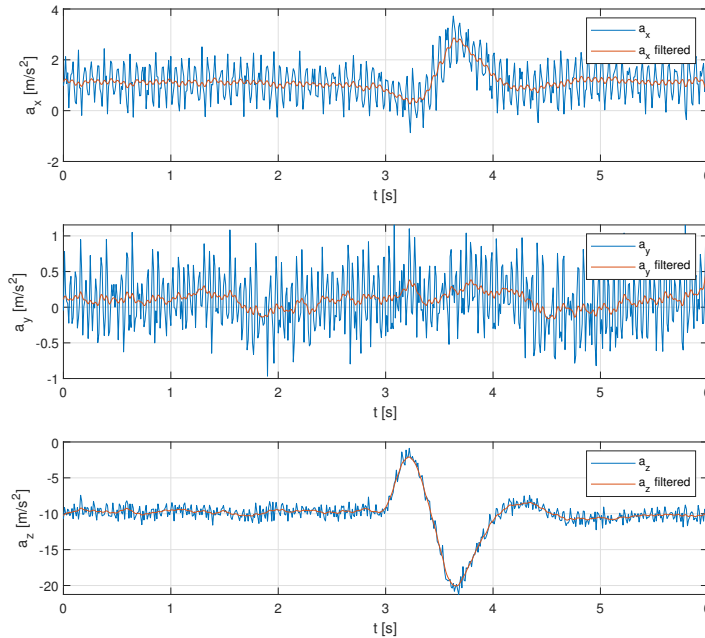
Parametar	Vrijednost
X_e	≈ 950 N
Y_e	0 N
Z_e	0 N
L_e	≈ -230 Nm
M_e	≈ -100 Nm
N_e	≈ -3 Nm

Korekcije podataka

Prije izračuna aerodinamičkih koeficijenata, podaci iz leta trebaju biti dodatno korigirani te pojedine greške senzora umanjene. Prvo, podaci s inercijske jedinice korigirani su za instalacijski kut inercijskog mjernog uređaja. Zatim, vrijednosti izmjerene na poziciji mjernog instrumenta, koja se ne podudara sa pozicijom težišta aviona, korigirane su za tu razliku između pozicije težišta i pozicije mjernog instrumenta. Primjer za korekciju ubrzanja izmjerenih inercijskom jedinicom dan je jednadžbom:

$$\begin{aligned}
 a_x &= a_x^{IMU} + (q^2 + r^2)x_{IMU,CG} - (pq - \dot{r})y_{IMU,CG} - (pr + \dot{q})z_{IMU,CG} \\
 a_y &= a_y^{IMU} - (pq + \dot{r})x_{IMU,CG} + (p^2 + r^2)y_{IMU,CG} - (qr - \dot{p})z_{IMU,CG} \\
 a_z &= a_z^{IMU} - (pr - \dot{q})x_{IMU,CG} - (qr + \dot{p})y_{IMU,CG} + (p^2 + q^2)z_{IMU,CG}
 \end{aligned} \tag{0.1}$$

gdje su $[a_x, a_y, a_z]$ i $[a_x^{IMU}, a_y^{IMU}, a_z^{IMU}]$ ubrzanja na poziciji težišta i inercijskog uređaja. Razlika između pozicije težišta i inercijskemjerne jedinice je $[x_{IMU,CG}, y_{IMU,CG}, z_{IMU,CG}]$. $[p, q, r]$ su kutne brzine a $[\dot{p}, \dot{q}, \dot{r}]$ derivativi kutnih brzina. Nakon toga, neki od parametara su filtrirani radi umanjenja šuma i smetnji mjernih instrumenata (slika 0.5).



Slika 0.5: Izmjerena i filtrirana linearna ubrzanja za jedan kratkotrajni manevar

Na kraju, korigirani su i podaci o struji zraka (napadni kut α , kut klizanja β , statički p_s i dinamički tlak q_c te brzinu strujanja TAS). Prvo, vrijednosti su korigirane za greške nastale strujanjem zraka oko samog mjernog uređaja i aviona. To je učinjeno postupkom rekonstrukcije putanje leta kojom su razvijeni modeli grešaka senzora. Tim modelima ispravljaju se izmjereni podaci. Primjer jednog modela za izmjereni napadni kut α_m dan je slijedećom jednadžbom:

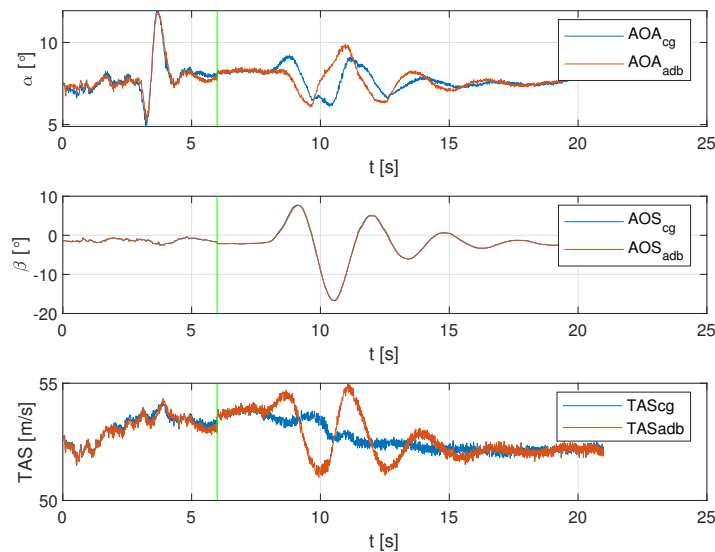
$$\alpha_{corr} = (\alpha_m - b_\alpha)/k_\alpha \quad (0.2)$$

gdje su:

$$b_\alpha = -0.1$$

$$k_\alpha = 1.8$$

a α_{corr} je korigirani napadni kut. Podaci o struji zraka su još dodatno korigirani za poziciju mjernog uređaja koja se ne podudara sa pozicijom težišta, slično kao i ranije. Slika 0.6 prikazuje podatke o struji zraka na poziciji mjernog uređaja *adb* te korigirane vrijednosti tj. na poziciji težišta *cg*, za jedan kratkotrajni manevar i jedan spregnuti mod skretanja i valjanja (*dutch-roll* manevar).



Slika 0.6: Korekcije podataka za poziciju težišta za jedan kratkotrajni manevar i jedan *dutch-roll* manevar

Procjena parametara

Nakon izračuna aerodinamičkih koeficijenata, osnovnim formulama, može se krenuti na procjenu parametara linearnom regresijom. Procjena parametara je započeta sa osnovnim modelima koji se mogu pronaći u svakoj knjizi dinamike leta npr. [3]. Nakon toga, modeli su postepeno poboljšavani uvrštavajući utjecaje drugih parametara. Tako je model koeficijenta momenta propinjanja nadograđen sa utjecajem koeficijenta potiska:

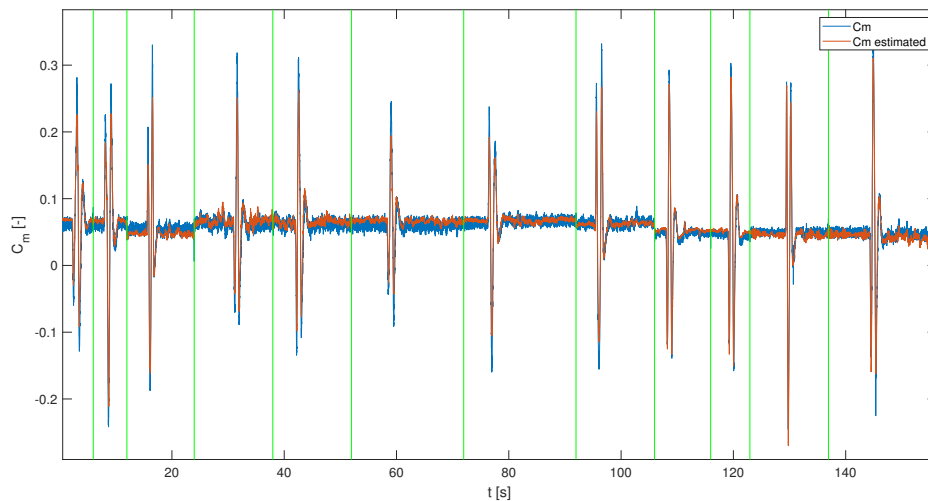
$$C_m = C_{m0} + C_{m\alpha}\alpha + C_{mq}q^* + C_{m\delta_e}\delta_e + C_{mC_T}C_T \quad (0.3)$$

sa parametrima navedenim u tablici 0.4.

Tablica 0.4: Procijenjeni parametri modela koeficijenta momenta propinjanja

Parameter	Value
C_{m0}	0.093118
$C_{m\alpha}$	-0.014379
C_{mq^*}	-16.429
$C_{m\delta_e}$	-0.039408
C_{CT}	0.36746

Podudaranje procijenjenog koeficijenta momenta propinjanja sa koeficijentom izračunatim iz izmjerenih podataka, vidi se na slici 0.7 za niz kratkotrajnih manevara.

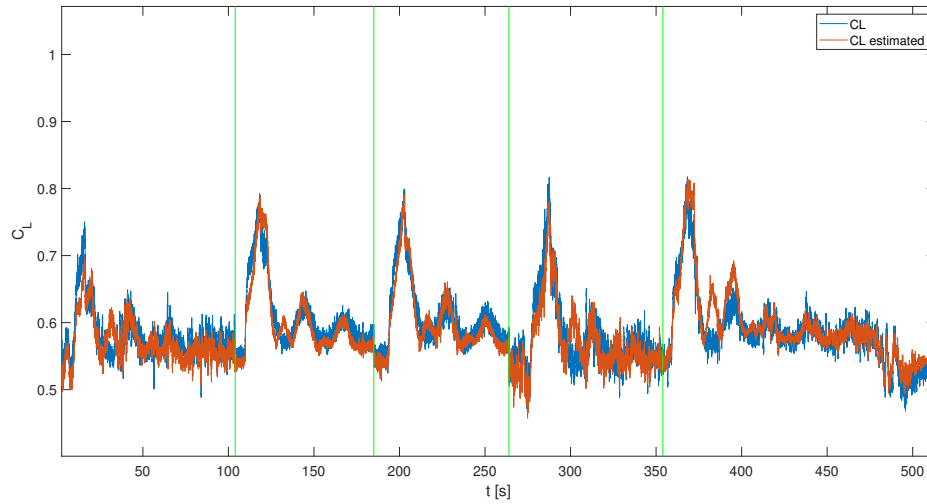


Slika 0.7: Linearna regresija koeficijenta momenta propinjanja za niz kratkotrajnih manevara

Unaprijeđeni model koeficijenta sile uzgona razvijen je kao:

$$C_L = C_{L0} + C_{L\alpha}\alpha + C_{Lq}q^* + C_{L\delta_e}\delta_e + C_{LC_T}C_T \quad (0.4)$$

te se podudaranje procijenjene i izračunate vrijednosti može vidjeti na slici 0.8 za niz fugoidnih manevara.

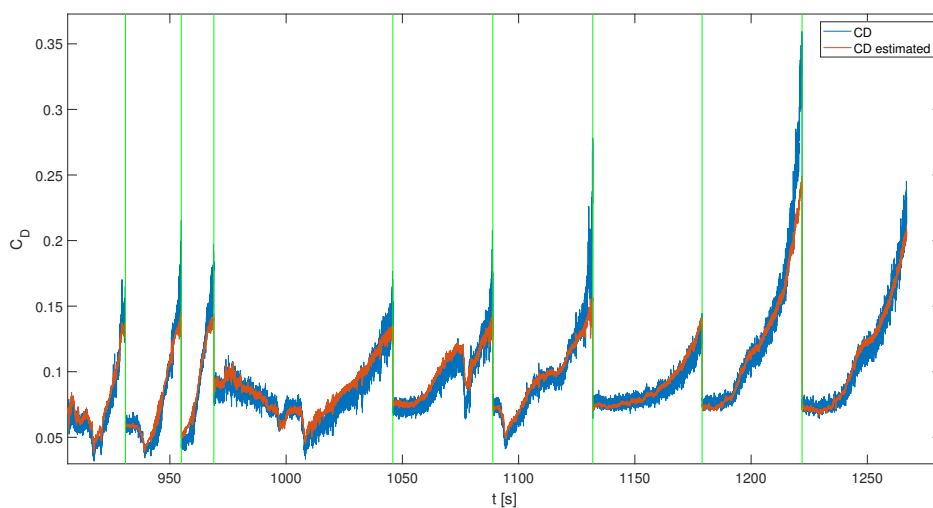


Slika 0.8: Linearna regresija koeficijenta sile uzgona za niz fugoidnih manevara

Model koeficijenta sile otpora je:

$$C_D = C_{D_0} + C_{D\alpha}\alpha + C_{DC_T}C_T \quad (0.5)$$

te se podudaranje može vidjeti na slici 0.9 za niz manevara sloma uzgona.



Slika 0.9: Regresija koeficijenta sile otpora za niz manevara sloma uzgona

Ovisnost koeficijenta sile otpora, kao i drugih koeficijenata, o kvadratu napadnog kuta $C_{D\alpha^2}\alpha^2$ je razmotrena ali rezultati time nisu znatno poboljšani. Budući da model mora biti što jednostavniji, kvadratna ovisnost o napadnom kutu nije uračunata.

Također su razvijeni osnovni modeli za koeficijente bočne sile, momenta valjanja i momenta skretanja.

Zaključak i budući rad

Ovaj diplomski rad je pisan kao nastavak na spomentuta dva prijašnja rada i kao osnova za neki budući rad na istom projektu. Stoga je pisan na način da se svaki budući čitatelj može lako snaći u tekstu, da su svi podaci i metode jasno prikazani te da se svaki dio rada može lako ponoviti korištenim sredstvima, dostupnim u priložima.

Ono što ostaje jest da se poboljšani podsustavi i metode, razvijeni u sklopu ovog rada, dodaju u postojeći PA-28 model u simulatoru zamijenjujući odgovarajuće stare podsustave. Budući rad također može uključivati i dodatan razvoj i poboljšanja svakog od podsustava. Tako bi se metode za procjenu mase i momenata tromosti mogle dodatno unaprijediti razvojem preciznijeg CAD modela. Model motora bi se također mogao dići na veću razinu bez potrebe za funkcijom za prilagođavanje ulaznih parametara. Modeli pogrešaka senzora su, u ovom radu, dovedeni na osnovnu razinu te bi se isto tako mogli znatno poboljšati. Na kraju, modeli aerodinamičkih koeficijenata su razvijeni linearnom regresijom dok se to može učiniti i puno kompleksnijim i točnijim metodama. To može uključivati regresiju polinomima višeg stupnja ili GAM metodu (*Generalized Additive Models*) kao što je to prikazano u [4].

1 Introduction

In the summer of 2019, the Center for Aviation (ZAV), at the Zurich University of Applied Sciences (ZHAW) conducted a flight test campaign on a Piper Pa-28-161 airplane, consisting of 159 test points flown through numerous manoeuvres.



Figure 1.1: Test aircraft Piper Pa-28-161 [2]

Since then, ZAV has the goal of a self-made model of a Piper PA-28 which can be implemented in their Research and Didactics Simulator (ReDSim) (figure 1.2). ReDSim was built in 2011 by employees and several students writing their project works. It's field of application contains research and development in flight dynamics and laboratory lectures providing an universal platform on which different aircraft and their configurations

can be flown.



Figure 1.2: ReDSim simulator at ZHAW

The aim is to have as good as possible simulator representation of the actual aircraft and the objective of this thesis is to get one step further in achieving that goal.

1.1. Aim and Scope of This Thesis

Since there are already two master projects [1] and [2], that dealt with mentioned flight test data, this thesis is supposed to be an extension to that work. These two previous thesis were mostly concentrated on performing the flight test campaign, flight test data gathering and processing as well as developing a base simulation model. In order to have a satisfying simulation model, a lot of different subsystems have to be developed and brought to the certain level of accuracy. This thesis is concerned with all the necessary data gathering and set up for a parameter estimation process determining aerodynamic coefficients. It is not supposed to provide comprehensive and exact models and parameters for aerodynamic coefficients but rather to set up a basis for the whole process of modelling along with some basic exemplary models. In the end, everything should be implemented in the ReDSim in a way that all the old subsystem, such as

engine model, mass and balance and aerodynamic model, are upgraded with the new models developed in the course of this thesis. This thesis is also written in a way that any future students working on this project can continue on this thesis and carry on upgrading the simulation model based on the set up made in this project.

1.2. Structure of the Thesis

This thesis is structured in the same way as the work flow that was followed during this project. That being said, following paragraphs provide a brief overview of this work.

Section 2.1. provides a brief overview of the flight test data, instrumentation and test points with some challenges that have to be mentioned before the data can be used for parameter estimation. Further in section 2.2., a brief introduction to system identification and parameter estimation in flight mechanics is given.

Following section 3. introduces test aircraft, measurement instrumentation and the whole process of flight test data preparation and processing.

Section 4. is dealing with mass, balance and inertia estimation necessary for all following calculations. With defined mass and balance, section 5. is describing the engine model and obtaining engine forces and moments needed for aerodynamic coefficient calculation.

Next, section 6. is showing some additional data corrections as well as some final data calculation along with the Flight Path Reconstruction (FPR).

Finally, section 7. is presenting the aerodynamic coefficient calculation followed by the basic parameter estimation, regression and modelling in section 8.. In the end, a brief discussion and conclusion is given in section 9.

All the code is written in MATLAB while the models are constructed with Simulink. Scripts, functions and other used utilities, developed throughout this work, can be found attached in appendices A., B., C.

2 Theoretical Background

2.1. Flight Test Data

Flight Test Data (FTD) is acquired during the flight test campaign, performed in 2019, and described in [2] and [1]. Flight test were performed on a Piper PA-28-161 Warrior III trainer airplane. Around 160 test points were flown through nine test flights composing of manoeuvres listed below.

2.1.1. Manoeuvres

The flight manoeuvres conducted for the system identification process are the ones that excite the dynamic motion of the aircraft. Measured flight test data then is used for developing and calculating parameters required by flight simulation models. A manoeuvre usually starts from a trimmed condition and is performed in a calm atmosphere. It is excited either as a pulse, single step, multi-step or a harmonic input. Actual manoeuvres performed during the flight test campaign of the PA-28 are:

- Short Period Pitch Oscillation
- Phugoid
- Dutch Roll
- Steady Heading Steady Sideslip
- Level turns

- Bank-to-bank roll
- Spiral check
- Stall
- Takeoff, landing and go-around

2.1.2. Instrumentation and Sensors

The aircraft was instrumented during the flight test campaign, in [2] and [1], and parameters were measured with:

- **Air Data Boom (ADB)** measuring Angle of Attack (AoA), Angle of Sideslip (AoS), static pressure and total pressure.
- **Inertial Measurement Unit (IMU)** measuring linear accelerations and rotational rates in three axes as well as the GPS position. Derived quantities such as the attitude angles were also available from the unit.
- **Propulsion system instrumentation** that recorded power setting i.e. throttle lever position and the propeller angular velocity (RPM).
- **String potentiometers** for control surface deflections, namely elevator, aileron and rudder deflections as well as their respective trim tab deflections.
- **Temperature sensors** measuring Outside Air Temperature (OAT) i.e. True Air Temperature (TAT) and a **hygrometer** sensor for the humidity level.
- **Stick force sensors, marker switch, video camera and sound recorder**

More detailed description of the instrumentation and its installation can be seen in in [2] and [1].

2.1.3. Issues with Flight Test Data

Due to the fact that this thesis is dealt with real, measured experimental data, certain complications arise due to the following reasons:

- Presence of sensor errors and measurement noise
- Modelling errors
- Atmospheric turbulence

Problems with atmospheric turbulence, in the scope of this thesis, are not dealt with under assumption that all the test flights were performed on proper days with low atmospheric turbulence and neglectable wind conditions. Modelling and its errors will be addressed more in the section 8. so it is left to describe some problems with the measurement instrumentation and sensors.

All measurement systems, although carefully calibrated, have their own errors. Since parameter estimation methods require data to be as accurate as possible, these errors must be corrected. Specifically in this thesis and its flight test data, the errors of the ADB are the only ones needed to be corrected. There is also measurement noise that is reduced with filters, like it is closely defined in section 6.2.

The ADB has two main sources that are causing data errors. One is the structure of the ADB itself, that changes the airflow around the ADB sensors. The other is the position error which accounts for the flow changes around the whole aircraft. The ADB can not always be placed in free stream conditions. Also it is subjected to the influence of aircraft movement which can result in significant errors to the AoA, AoS and dynamic pressure i.e. True Air Speed (TAS). First error is removed by ADB calibration in the wind tunnel which was done in the scope of preceding master thesis [2]. Elimination of the second stated error, along with reducing the first one, is done with the process of Flight Path Reconstruction (FPR). This process is described in section 6.4.2. There are many other ways of dealing with the measurement errors, like using extended Kalman filters or output-error method ([3]). Although these methods can be more accurate, they are more exhaustive too.

Another issue is the uncertainty in fuel mass distribution. Fuel level was recorded only for the total amount of fuel, not specifying the fuel in each wing. Since fuel mass per wing depends on the aircraft attitude and has an effect on the Center of Gravity (CG) position and mass moments of inertia, this introduces a serious issue as uncertainty of

mass distribution along the lateral axis. This directly contributes to the errors in the estimation of aerodynamic coefficients that are very hard to correct.

2.2. System Identification and Parameter Estimation

When talking about system identification, we are describing a complex process of representing real physical processes with simplified physical systems and mathematical models. Specifically the development of a mathematical model using experimental data is called *system identification*. This concept is shown in figure 2.1 where a control surface deflection δ , representing a system input u , is acting on both the real dynamic system S and a representation of that system, being the simulation model M . Output y from both can later be analysed and compared.

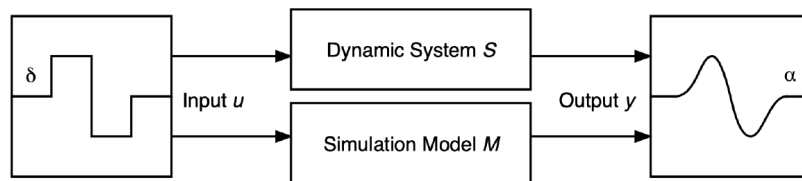


Figure 2.1: System identification scheme [1]

The output of the mathematical simulation model M should ideally be the same as the measured aircraft response (output of the dynamic system S). In flight dynamic systems that is almost never the case. While the output of the mathematical model is defined by the implemented simulation model, output of the dynamic system is actually the aircraft's response i.e. measured flight test data.

While the real dynamic system input can be directly recorded with the measurement instrumentation, aerodynamic forces and moments, as an output quantities, have to be derived from other related measured parameters like linear and angular accelerations or flow angles. Since measurement data is subjected to experimental uncertainties it has to be corrected and statistically estimated. This process of quantification of the parameter values is called *parameter estimation*. As it can be seen, these processes of parameter

estimation, system identification and simulation are greatly intertwined, connected and often iterative (figure 2.2.).

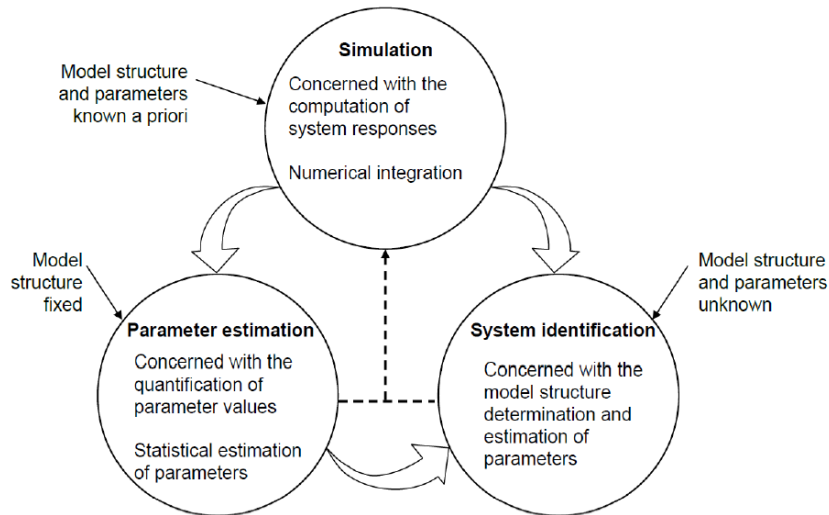


Figure 2.2: Definition of system identification, parameter estimation and simulation [3]

System identification of aerodynamic models is, as defined in [3], taken out through the "Quad-M" methodology:

- Manoeuvre
- Measurement
- Method
- Model

Each of the four Ms must be carefully investigated to achieve the desired model (figure 2.3). This starts by selecting or designing *manoeuvres* that excite the desired modes of the aircraft. These manoeuvres need to be distributed throughout the flight envelope so that they contain the information to build the desired model. The *measurement* system and filters need to be carefully selected. This includes determining the signals to be measured, the required range, accuracy and sampling rates, the characteristics of filters, the method of calibration and so on. Selecting an appropriate *model* structure is driven,

as are all the other Ms too, by the requirements of the model. The last M is the choice of the *method*, which needs to be selected according to the data quality and the selected model structure to generate the desired results. The individual Ms in the "Quad-M" are strongly interdependent and therefore cannot be treated independently ([3]).

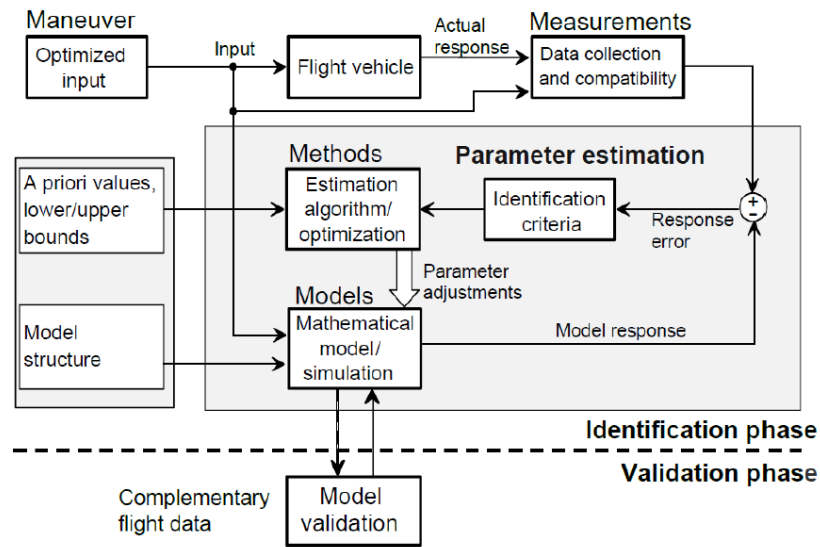


Figure 2.3: "Quad-M" methodology [3]

2.3. Conventions

The following (figure 2.4) conventions are followed throughout this thesis:

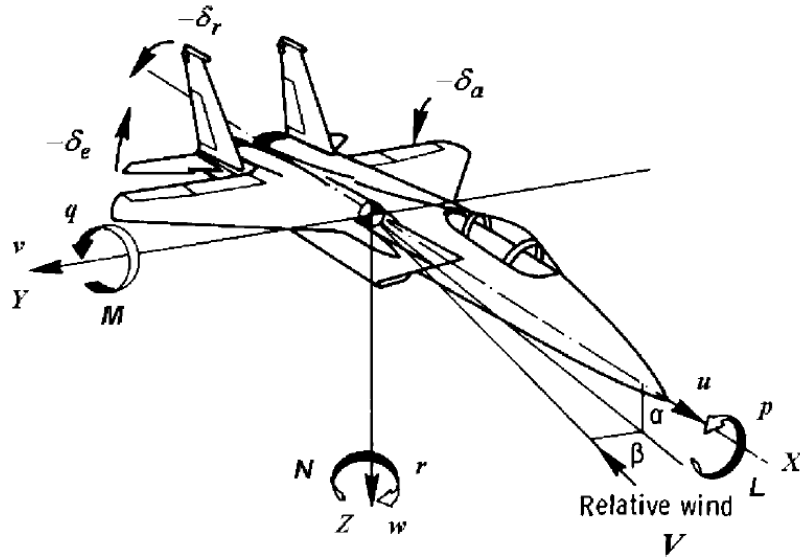


Figure 2.4: Axis, moments and angle definition [5]

where L , M , N are positive moments caused by negative control surface deflections defined in table 2.1.

Table 2.1: Control surface deflections convention

Symbol	Description	Comment
δ_e	Elevator deflection	Positive deflection is elevator down
δ_a	Aileron deflection	Arithmetic mean of both aileron deflections, positive deflection is aileron up
δ_r	Rudder deflection	Positive deflection is the rudder to the left

Coordinate system shown on the figure 2.4 is also called Body Coordinate System (BCS).

3 Flight Test Data Preparation

3.1. Test Aircraft

Piper Pa-28-161 Warrior III aircraft is a single-engine, two-blade fixed pitch propeller and fixed gear monoplane. It is further equipped with the installed measuring instrumentation stated in section 2.1.2. the next section. The aircraft carries the registration HB-PRL with serial no. 2842292 and is owned by the *Aussenschweizerische Fluggemeinschaft (ASFG)*, located in Wangen-Lachen, Switzerland.



Figure 3.1: Test aircraft HB-PRL, Piper Pa-28-161 Warrior III [1]

Some of the aircraft's general dimensions, used in this work, are presented in table 3.1 while aircraft geometry is illustrated in figure 3.2.

Table 3.1: General dimensions of the PA-28

Dimension	Value
Wingspan b	10.67 m
Wing root chord length c_r	1.60 m
Wing tip chord length c_t	1.07 m
Mean aerodynamic chord \bar{c}	1.602 m
Wing surface reference area S_{ref}	15.8 m ²
Wing aspect ratio AR	7.24

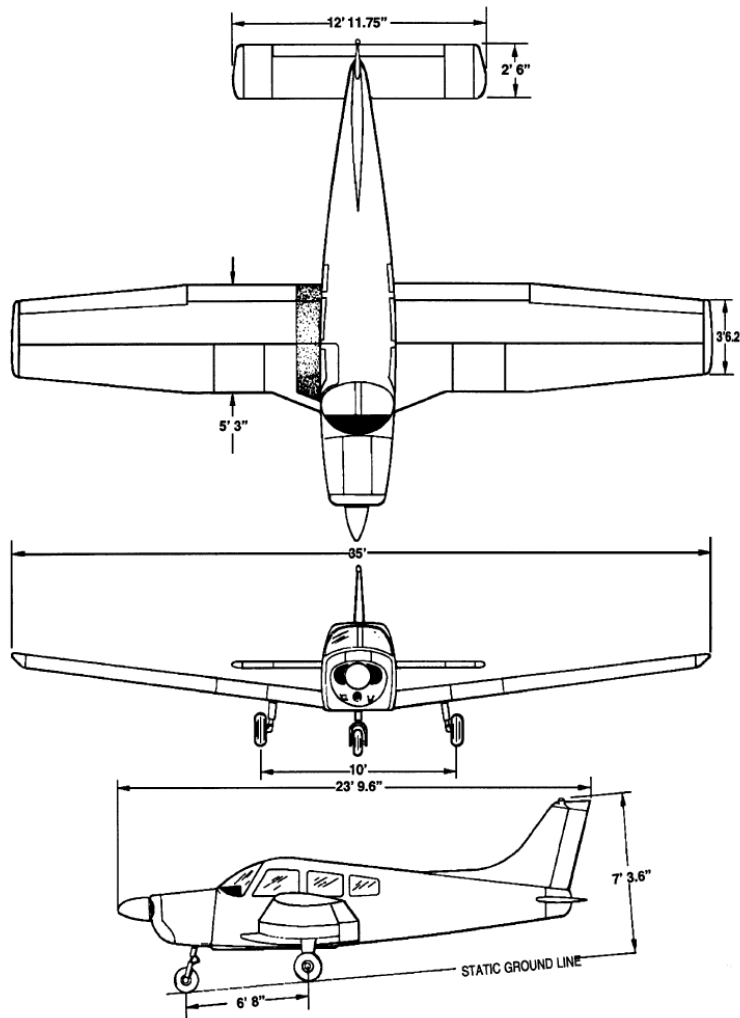


Figure 3.2: Top, front and side view of the test aircraft [6]

3.1.1. Aircraft Configurations

With the standard configuration described in Pilot's Operating Handbook (POH) [7], aircraft was equipped with measurement instruments specified in 2.1.2. Changes to configuration were result of the aircraft's mass and balance loading, flaps deployment, and engine power settings. All flight tests started with the same aircraft mass loading of ≈ 1008 kg while the CG position was either forward at 2.25 m or aft at 2.32 m measured from the propeller tip (calculated during the aircraft weighting in [1], also section 4.3.). The CG in percentage of mean aerodynamic chord \bar{c} was either 16.2% in the forward or 20.3% in the aft configuration, as calculated in [1]. The engine power settings were sectioned in four categories: idle power, low, trim and high power (i.e. aircraft trimmed for 70 kt (≈ 130 km/h), 80 kt (≈ 148 km/h) and 95 (≈ 176 km/h) kt). With the exception of take off, landing and go-around, the flaps remained retracted. All flight manoeuvres were conducted within the limitations stated in the POH [7].

3.2. Data Acquisition

Data acquisition system is made of two units: the IMU (figure 3.3) which logs inertial data and GPS position and the cRIO that recorded the remaining parameters like the ADB quantities, temperatures and control surface deflections. Both unites were installed in the baggage compartment of the aircraft (figure 3.4).



Figure 3.3: Ekinox 2, IMU from manufacturer SBG Systems [2]

The IMU is equipped with three tactical grade Micro-Electro-Mechanical-Systems (MEMS) gyroscopes that measure angular rates and three MEMS capacitive accelerometers for the linear accelerations. Along with the IMU, two GPS antennas, to track the GPS, are mounted on the top of the fuselage. The IMU itself is, as already stated, mounted in the baggage compartment but for the purpose of future calculations, IMU position in Aircraft Coordinate System (ACS) is needed:

$$x_{IMU} = 3.39 \text{ m}$$

$$y_{IMU} = 0 \text{ m}$$

$$z_{IMU} = -0.216 \text{ m}$$

Aircraft coordinate system is defined in section 4.2. while the procedure of acquiring the IMU position is described in appendix C.1.

The cRIO contains seven A/D converters (figure 3.4), which the sensors are connected to, logging the data onto an internal storage. A/D converters, also called C-Modules, are connected to different sensors recording the data with different sampling rates, depending on the sensor purpose or limitations by the hardware/software. RPM is then recorded with the sampling frequency of 10000 Hz, temperature with 5 Hz, stick forces with 1612.9 Hz while control surface deflections with 100 Hz.

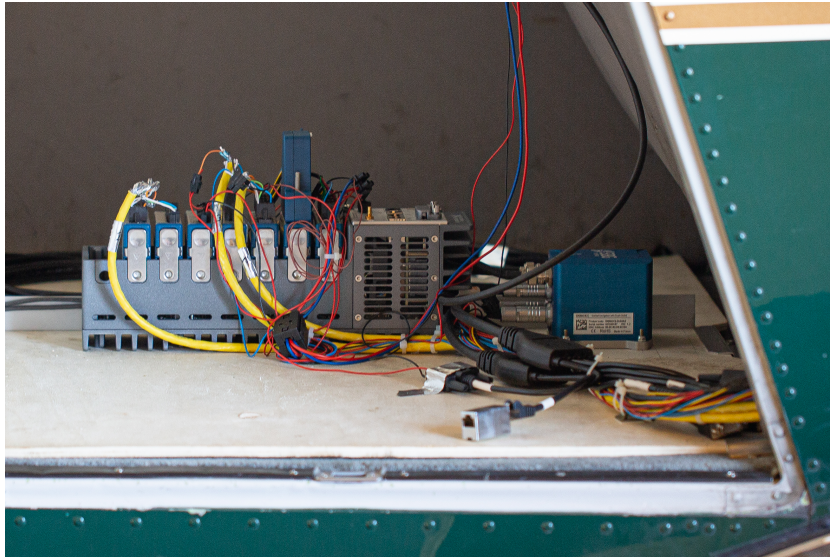


Figure 3.4: IMU and cRIO with its 7 C-modules mounted in baggage compartment [2]

In order to synchronize the data between the IMU and cRIO, an electric circuit connecting the battery, a marker switch, the IMU and the cRIO is installed. Marker switch was triggered by the Flight Test Engineer (FTE) during the flights, marking different manoeuvres and flight segments. Triggering of the switch was recorded by both the IMU and the cRIO allowing the data synchronization in the post processing.

3.3. Data Processing

Following data gathering with the IMU and cRIO, flight test data has to be properly processed. Data processing was already done in [2] but due to some inconsistencies it had to be reprocessed in slightly different way. Processing procedure, developed in [2], is still closely followed and it will be presented in a similar manner (figure 3.5). First, the data has to be collected and corrected for certain filter delays. Afterwards, it has to be synchronized and, if necessary, resampled to 100 Hz. Next, signal values have to be converted to measurement values and some quantities have to be corrected with sensor error models. Last is to add some calculated values and cut the data into manoeuvres.

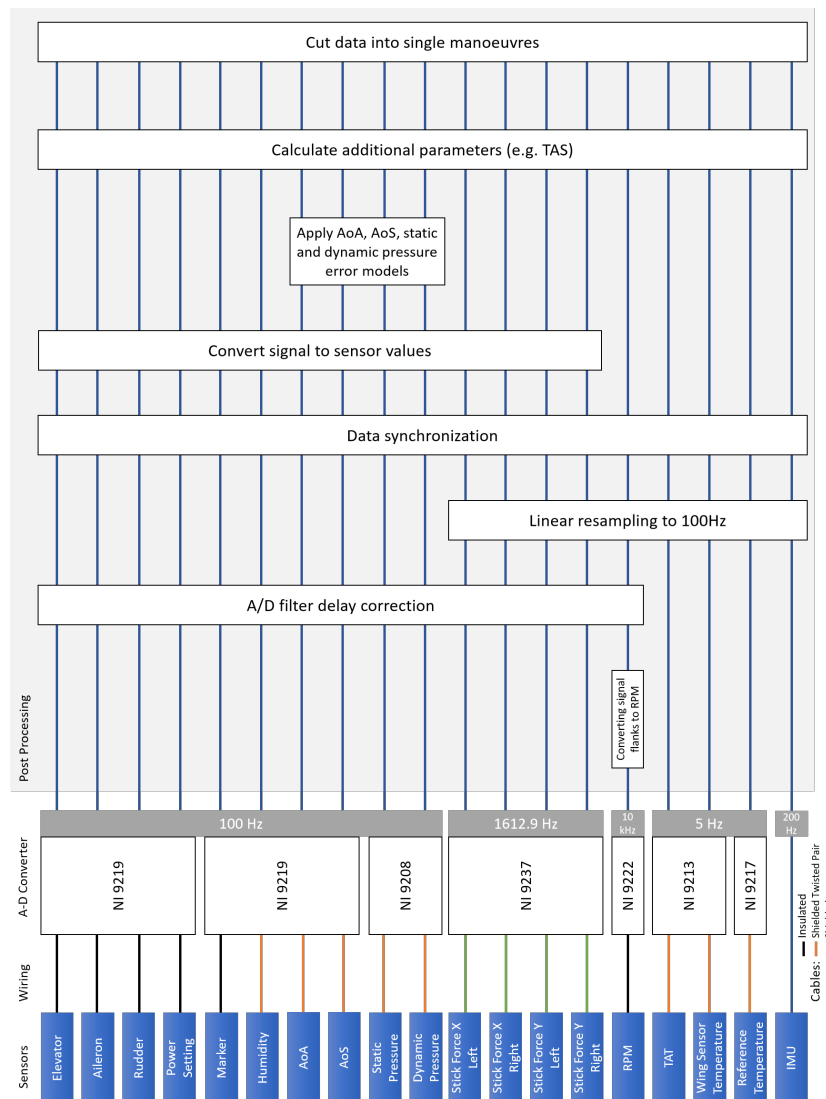


Figure 3.5: Data processing overview [2]

For the readers that would like to access the processing scripts and functions along with other utilities, all files can be found in appendix A.

3.3.1. Data Collection

Since data was collected in the preceding master thesis, it was here adopted as it was. IMU data comes in three different files in the ASCII format. One contains inertial data with the IMU itself set as a reference while the other is the inertial data

with the ADB set as a reference. Third file is the marker data. cRIO data is as well adopted in ASCII format in 4 different files, each representing different sampling rates. Two additional files had to be made, in the scope of this thesis, for the purposes of data reprocessing. One with start times of each of the four cRIO files and one with the synchronization data. All the data is imported, gathered and processed with the MATLAB function *processData.m* available in appendix A.1.2. Flight test data is also available in appendix A.1.1.

3.3.2. Delays and Synchronization

First, cRIO data had to be corrected for the delays introduced by the C-Modules. Each A/D converter, except the NI 9222, comes with a noise rejection filter that entries a delay to the sensor data. Delays are calculated in [2], from where they have been taken over and applied in reprocessing procedure. After that, all the data had to be re-sampled to 100 Hz for the synchronization between the IMU and the cRIO to be possible.

Data is synchronized with the help of the marker switch. When triggering the switch, time stamps were logged to the cRIO and the IMU. Using these time stamps the two sets of data are connected to the same time reference. Since the cRIO had different time reference, that was off by 2 hours, IMU (GPS) time was set as a reference. Also, this 2 hours shift had to be incorporated to the cRIO data and that was done with the excel file *8_cRIO_StartTimes_....xlsx*, attached in appendix A.1.1., containing cRIO start times (-2 hours). Another excel file, *9_synchronization_....xlsx*, containing synchronization information is present in the same appendix.

3.3.3. Calibration

Next, it is necessary to convert the signal values to the measurement values. That is done with the calibration values either specified by the manufacturer, or calculated in the preceding thesis [2] and [1]. Again values of offset and gain, presented in [2], are taken over from the previous works and applied again here in this thesis while reprocessing. Some conversion quantities are presented in table 3.2.

Table 3.2: Some data calibration values taken from [2]

Sensor	Gain	Offset	Signal	Unit
Static pressure	3125000.0	57500.0	[A]	[Pa]
Dynamic pressure	313743.0	-1267.5	[A]	[Pa]
AoA	668.8	-40.3	[V]	[deg]
AoS	184.1	-49.7	[V]	[deg]
Elevator	-89.9	-10.2	[V]	[deg]
Rudder	286.0	21.1	[V]	[deg]
Power setting	-383.7	-61.9745	[V]	[%]
Relative humidity	0.1	0	[V]	[%]
TAT	1.0	273.15	[°C]	[K]

3.3.4. Sensor Error Models

What is left is to correct the ADB measured signals i.e. AoA, AoS and the pressures. As stated in section 2.1.3., due to the air flow velocity around the ADB, data is subjected to sensor errors so it is necessary to correct it. Error of the ADB itself is corrected with the error models developed during the ADB calibration in the wind tunnel in [2]. It is important to mention that the position error and pressure lag of the ADB are not corrected with these models but rather later in the FPR (section 6.4.2.). Sensor Error models are taken from the preceding master thesis [2] where one can see them in details and how they are developed. Here, only the AoS sensor error model is presented:

$$\beta_{corr} = b_{\beta} + K_{\beta} \cdot \beta + K_{\alpha} \cdot \alpha + K_{q_c} \cdot q_c + K_{\alpha\beta} \cdot \alpha\beta + K_{\alpha^2} \cdot \alpha^2 \quad (3.1)$$

where β_{corr} is the corrected angle of sideslip, α and β are the measured AoA and AoS, q_c is the measured dynamic pressure and the rest are the estimated parameters:

$$\begin{aligned}
b_\beta &= 0.32 \\
K_\beta &= 0.96 \\
K_\alpha &= -0.0017 \\
K_{q_c} &= -0.00021 \\
K_{\alpha\beta} &= 0.00037 \\
K_{\alpha^2} &= 0.000094
\end{aligned}$$

AoA, static and dynamic pressure are corrected in the same manner.

3.3.5. Calculations

Final step is to add some calculated parameters to the test data. These are calculated directly from the measured and converted/corrected values. First, the air density is defined as:

$$\rho = \frac{p_s}{(R \cdot T)} \quad (3.2)$$

where p_s is the measured static pressure corrected with the ADB error model stated in the previous section. T is the outside air temperature directly measured with the thermocouple sensor and $R = 287.058 \text{ J kg}^{-1} \text{ K}^{-1}$ is the specific air molar mass. True airspeed TAS is calculated with corrected dynamic pressure q_c :

$$TAS = \sqrt{\frac{2q_c}{\rho}} \quad (3.3)$$

Also, Pressure Altitude (PA) is calculated as:

$$PA = 145366.45 \cdot \left(1 - \left(\frac{p_s}{1013.25}\right)^{0.190284}\right) \cdot 0.3048 \quad (3.4)$$

where 0.3048 is a conversion factor from feet to meters.

3.3.6. Cutting Data to Manoeuvres

In the end, data has to be properly cut from the whole flights into manoeuvres. Using the marker data and the notes from the flight test cards, appendix A.1.1., developed during the flight test campaign in [2] and [1]. In this step, information about trim and fuel level is added to the data. Manoeuvre data is saved to files with a descriptive name as shown in table 3.3.

Table 3.3: Naming convention of the manoeuvre data files

Name	Values	Description
FID_	[1...16]	Flight ID
MID_	[1...1015]	Manoeuvre ID
CG_	FWD,AFT	CG position category
Mass_	M	Aircraft mass category
Alt_	L,M,H	Initial altitude category
S_	L,M,H	Initial speed category
P_	L,M,H	Initial power category
Mnvr_	SHSS, Phugoid...	Manoeuvre name

When looking at the plots containing more than one manoeuvre data, manoeuvres are, throughout this work, separated with the green line (marking the breakpoints between different manoeuvres). The example is presented on figure 3.6, showing true airspeed *TAS* for a stall, phugoid, dutch roll and steady heading steady sideslip manoeuvre.

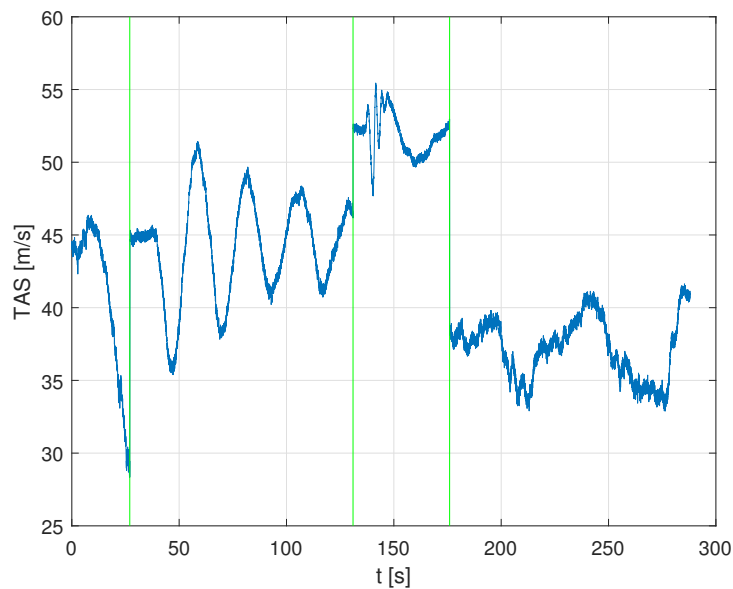


Figure 3.6: True airspeed *TAS* for a stall, phugoid, dutch roll and steady heading steady sideslip manoeuvre

3.3.7. Data Structure

Finally, after the whole data processing procedure, FTD comes as a structure divided in three parts: data from the IMU (with the prefix *imu*), data from the cRIO (prefix *crio*) and the calculated data (*calc*). IMU data is again separated in two parts with one being the data with the IMU as a reference while the other is the same data but with the reference at the ADB. Data from the cRIO comes in three parts: raw sensor data (with the suffix *raw*), signal data converted into measurement data that still has to be corrected (suffix *conv*), and signal data converted into measurement data that is either corrected or does not need any correction (*corr*). Flight test data structure is presented in table 3.4.

Table 3.4: Final data structure with all the parameters from flight test campaign

Parameter	Source	Signal remark	Unit
GPS time and date	IMU		[DD.MM.YYYY hh:mm:ss.SSS]
Roll, pitch and yaw angle ϕ, θ, ψ	IMU		[deg]
Linear accelerations a_x, a_y, a_z	IMU		[m/s ²]
Total acceleration	IMU		[m/s ²]
Rotational rates p, q, r	IMU		[deg/s]
Total rotational rate	IMU		[deg/s]
Linear acceleration x,y,z	IMU	g-compensated	[m/s ²]
GPS altitude	IMU		[m]
GPS latitude, longitude	IMU		[deg]
Linear accelerations x,y,z	IMU	ADB reference	[m/s ²]
Total acceleration	IMU	ADB reference	[m/s ²]
Linear accelerations x,y,z	IMU	ADB reference, g-compensated	[m/s ²]
Outside air temperature T	cRIO	raw, corr	[K]
Wing sensor temperature	cRIO	raw, corr	[K]
Relative humidity	cRIO	raw, corr	[%]
AoA, AoS α, β	cRIO	raw, conv, corr	[deg]

Aileron deflection δ_a	cRIO	raw, corr	[deg]
Elevator deflection δ_e	cRIO	raw, corr	[deg]
Rudder deflection δ_r	cRIO	raw, corr	[deg]
Power setting	cRIO	raw, corr	[%]
Static pressure p_s	cRIO	raw, conv, corr	[Pa]
Dynamic pressure q_c	cRIO	raw, conv, corr	[Pa]
Stick force sensors	cRIO	raw, corr	[N]
Propeller RPM	cRIO	raw, corr	[1/min]
Air density ρ	cRIO	calc	[kg/m ³]
True airspeed TAS	cRIO	calc	[m/s]
Pressure altitude PA	cRIO	calc	[m]
Trim	cRIO	added	[-]
Fuel	cRIO	added	[USG]

Also, attached in appendix [A.1.2.](#), there is a function *organizeData.m*, developed in the scope of this thesis, that organizes the data based on the user input. Only the selected data variables are kept and properly renamed removing all the prefixes and suffixes and assigning them more descriptive names needed for the purposes of future analysis.

4 | **Mass, Balance and Inertia**

For any further calculations, it is necessary to have aircraft mass distribution, its center of gravity (CG) position and mass of moments of inertia. CG position is later used to calculate engine forces and moments as well as IMU and ADB offsets from CG while mass and inertia, along with CG position, are needed for aerodynamic coefficients calculation in section 7. Many calculations in this chapter depend on the references and methods in which the units are not SI based. These were calculated, and presented here, with the original units and later converted to SI units.

4.1. Mass Estimation

Since all of the manufacturer mass distribution data is unavailable, all of the mass values are based on the approximated values. First, aircraft sections mass distribution and Operating Empty Mass (OEM) of the aircraft are estimated and compared to the actual weighting of the aircraft. With so verified values, Aircraft Take Off Mass (ATOM) and actual aircraft mass, at every test point, is calculated.

All of the calculations and estimations are done with MATLAB scripts and functions which can be found in appendix [B.1](#).

4.1.1. Mass Distribution and OEM Estimation

Mass distribution estimation is taken over from the previous master thesis ([1]) where it is estimated in respect to the Cessna method presented in [8] which applies for small

and low performance aircraft with maximum airspeed of less than 200 kt [9]. That method is usually used in the preliminary design phase of aircraft development and includes several assumptions and simplifications. Even though it is done with respect to Cessna C172, PA-28-161 shows somewhat similar characteristics for the method to be reasonably applied.

Mass of the aircraft, as suggested by the *DATCOM* method (for moments of inertia calculation) in [10] is divided into six different structure mass groups: fuselage, wing, vertical and horizontal stabilizer, powerplant and undercarriage. The mass of fuel, cargo and flight crew has to be considered as well, even though these are the dynamic values.

In [1], ATOM is calculated by summation of the basic six structure mass groups with addition of constant baggage, crew and fuel mass. That was resulting in constant ATOM value. Since fuel level is changing throughout all the flight test points as well as crew configuration for different test flights, constant aircraft mass was not a good representation of the actual situation. That is why it was decided to first estimate OEM that is represented just by the six basic structural sections and later incorporate dynamic masses. This way, the computed actual mass of the aircraft, during every test point, corresponded to the actual mass of the test aircraft.

Mass of the measuring instrumentation is taken into account only by the baggage weight of 10 kg, corresponding to the data acquisition system (cRIO and IMU). Other measuring equipment such as ADB and the GPS antennas are not taken into account but their mass contribution is considerably smaller, compared to the rest of the sections.

4.1.2. Actual Mass of the Aircraft

With the OEM being defined, it remains to determine the masses that change during flight or during different test flights. First is the crew configuration that was changing on each test flight. Besides the pilot, that did not change through the whole flight test campaign, crew consisted of a Flight Test Engineer (FTE) as well. There were two different FTE's (with different masses) that were sitting either in the front (copilot) or in the back right seat (passenger). CG position was defined by the position of the FTE so when the FTE was sitting back, that corresponded with the aft CG position while forward CG was conditioned by FTE sitting in front. There is also FTE's laptop

and some additional equipment that was placed on the two remaining free seats in the aircraft. This equipment was also incorporated in the crew mass estimation where equipment on each seat represented the mass of a passenger. The mass of the equipment on each seat was equal to 1 kg.

Second variable mass is the remaining fuel. Fuel amount at take off was 34 USG for all the test flights. During test flights, FTE was recording the fuel level at the beginning of each manoeuvre. This way the fuel amount changes through the whole test flight but remains constant during each of the manoeuvres. Manoeuvre duration is anyway so short that the fuel level change is impossible to read from the instruments. Since there is no record of how much fuel there was in each wing, the assumption is that the amount of fuel in each wing was equal. That being said, the fuel sloshing effects are not taken into account. That can have effect on the inertia values during the lateral manoeuvres that will not be covered by this estimation. When working with fuel data, different conversions are used:

$$\text{USG to litres} = 3.7851/\text{USG}$$

$$\text{USG to lbs} = 5.99 \text{ kg/l}$$

$$\text{Avgas density} = 0.719 \text{ lbs/USG}$$

As already stated, baggage mass is 10 kg representing the measuring equipment in the baggage compartment.

That being said, Zero-Fuel Weight (ZFW) was calculated as:

$$\text{ZFW} = \text{aircraft weight} + \text{crew weight} + \text{baggage weight} \quad (4.1)$$

following with:

$$\text{Aircraft mass} = \text{ZFW} + \text{remaining fuel} \quad (4.2)$$

$$\text{ATOM} = \text{ZFW} + \text{fuel at take off (34 USG)} \quad (4.3)$$

In the end, both estimated OEM and ATOM corresponded with the actual mass of the aircraft, measured during the weighting of the aircraft (section 4.3.). That verified the mass distribution estimation, which could later be used to calculate moments of inertia.

4.2. Inertia and CG estimation

Starting point for inertia tensor and CG position determination were as well calculations presented in preceding master thesis [1]. CAD model (figure 4.3) is constructed, as well in [1], with the reference to the coordinate system defined by the Airplane Maintenance Manual (AMM) [6] and shown on the figure (4.1).

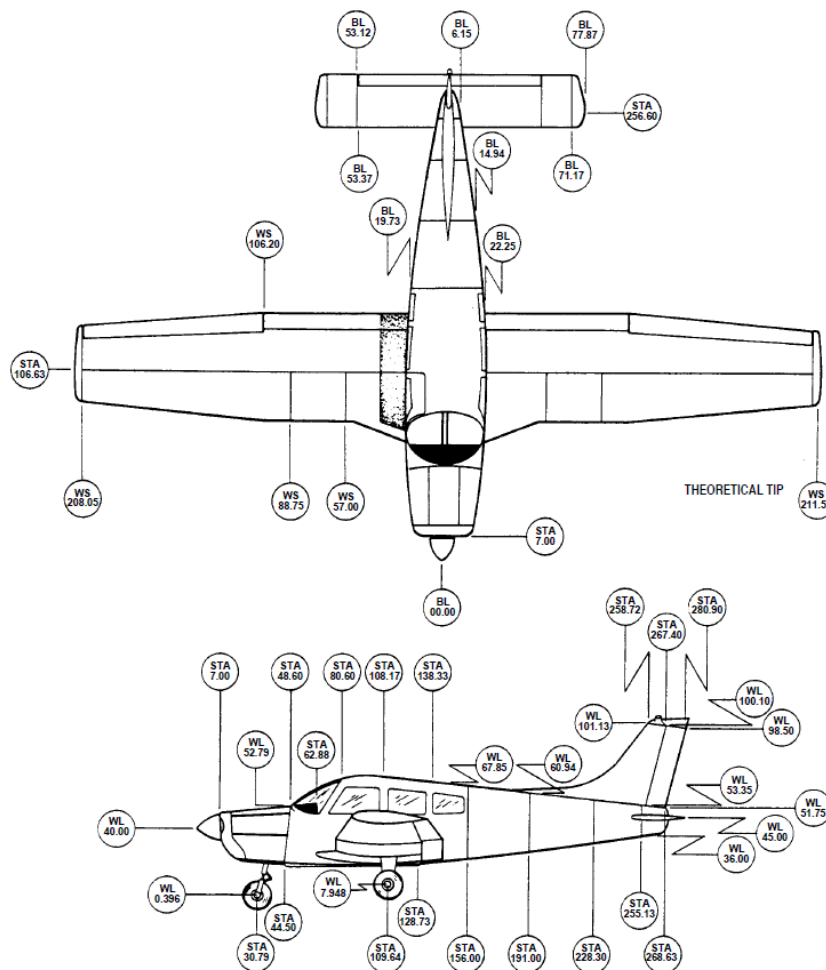


Figure 4.1: Station reference lines from AMM [6]

As suggested by *DATCOM*, remote axes were defined with an offset to the same aircraft reference stations shown on figure 4.1. As it can be seen in [1], remote axes were defined so that all the inertia moments of the major sections are positive and/or lie within the

plane of symmetry.

Another coordinate system that is used in this work is the one defined by the POH [7] and throughout this work will be called Aircraft Coordinate System (ACS). Orientation of the axes is the same as the one in the AMM but the x axis origin starts at propeller tip and goes through the fuselage (figure 4.2). CG position (as well as IMU and ADB position) is determined with the reference to ACS. One should take care while comparing the reference coordinates from the POH and AMM. While the datum of the aircraft coordinate system in POH (ACS) is at the propeller tip, AMM coordinate system origin is at the station 0 which is 2.2 in in front of the propeller tip.

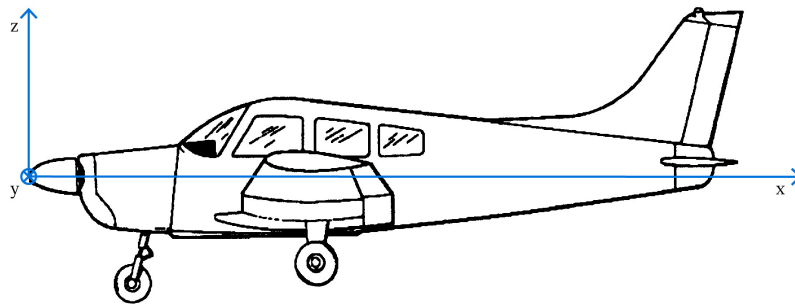


Figure 4.2: Aircraft coordinate system

4.2.1. Main Moments of Inertia

Main moments of inertia are calculated applying *DATCOM* method developed by the *United States Air Force (USAF)* [10]. This method determines main mass moments of inertia for each of the six structural sections, stated above, around their own centroids $I_{0x,0y,0z}$ as well as in respect to a remote axis system $I_{x,y,z}$. Sections are finally summed up to compute aircraft's main moments of inertia $I_{xx,yy,zz}$. This calculation is precisely shown in [1], where it is also, with some corrections, taken from.

All centroid locations, for the primary six sections, are defined from the CAD model. CAD model is also done in the scope of the preceding thesis where all the aircraft's sections are represented with simple symmetrical bodies (figures 4.3,4.4,4.5).

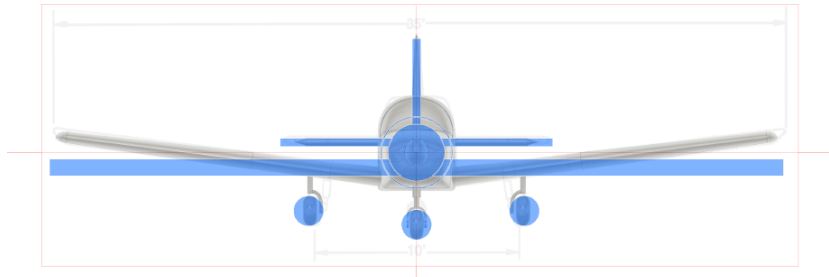


Figure 4.3: Front view of the basic reconstructed CAD model [1]

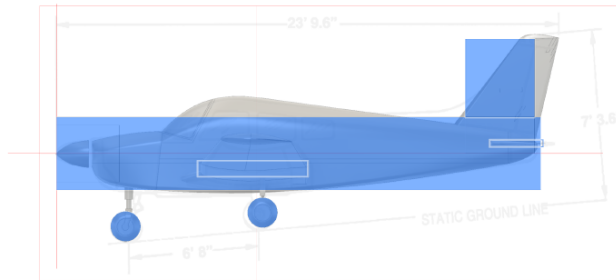


Figure 4.4: Left side view of the basic reconstructed CAD model [1]

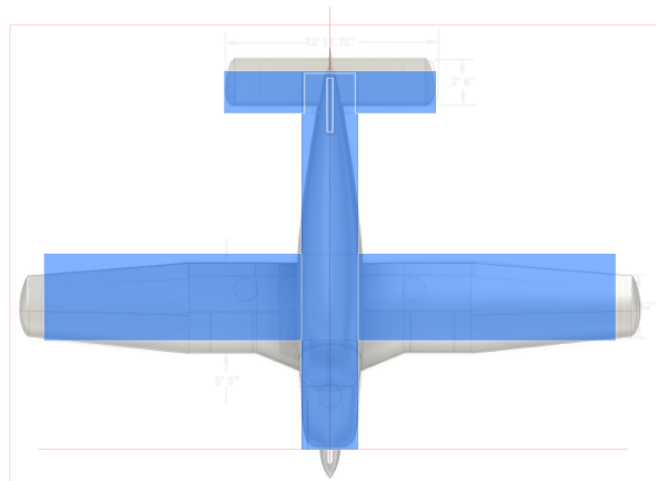


Figure 4.5: Top view of the basic reconstructed CAD model [1]

Centroid locations for baggage fuel and crew are partially taken from the POH while the rest is also defined by the CAD model. Each of these is represented with the symmetrical body (rectangular) as well.

Same like mass estimation in [1], moments of inertia calculation, in preceding master thesis, did not incorporate variable fuel and crew values. That is done as part of this work.

Fuel moments of inertia are calculated equally as in [1] with different fuel mass for different manoeuvres.

Crew members were in [1] simplified as rectangular bodies where pilot and copilot were represented by one rectangular and passengers with the other, both with the same dimensions:

$$\text{width} = 33 \text{ in}$$

$$\text{length} = 15 \text{ in}$$

$$\text{height} = 50 \text{ in}$$

This way it was not possible to take into account different FTE placement (front and back seat) and the difference between pilot and FTE weight. In this work, each crew member is represented with the same square body with the original width halved. That being done, each crew member is represented with its own square body that has its own centroid and results in its own moment of inertia. Crew configuration modification are now easy to implement and each one gives a slightly different result to the total moments of inertia.

It is important to say that this estimation is greatly simplified and does not take into account ADB, GPS antennas, and other measuring equipment apart from the one being already stated. Everything is done according to the simple CAD model with rudimentary geometrical shapes as aircraft sections.

4.2.2. Center of Gravity Position

With moments of each of the sections around the remote axes defined as:

$$\begin{aligned} M_{x_i} &= m_i x_i, \\ M_{y_i} &= m_i y_i, \\ M_{z_i} &= m_i z_i, \end{aligned} \tag{4.4}$$

where m_i is the mass of the section and x_i, y_i, z_i are the centroid distances from remote axes, CG position is relatively easy to compute as:

$$\begin{aligned} x_{CG} &= \frac{M_{x_{total}}}{m_{aircraft}} - x_0 \\ y_{CG} &= \frac{M_{y_{total}}}{m_{aircraft}} - y_0 \\ z_{CG} &= \frac{M_{z_{total}}}{m_{aircraft}} - z_0 \end{aligned} \tag{4.5}$$

where $M_{x_{total}}, M_{y_{total}}, M_{z_{total}}$ are the total moments around the remote axes and x_0, y_0, z_0 are the offsets from the remote axes to the aircraft coordinate system with the datum at the propeller tip.

4.2.3. Cross Moments of Inertia

Since *DATCOM* method does not provide calculations for cross moments of inertia, rough estimates are calculated by the use of ordinary equations available in any mechanics book such as [11] or [12]. They are estimated based on the same references and CAD model as the ones before, using calculated CG position. Cross moments of inertia for each defined section are computed as:

$$\begin{aligned} I_{xy_i} &= I_{Cx'y'_i} + m_i x_{C_i} z_{C_i} \\ I_{xz_i} &= I_{Cx'z'_i} + m_i x_{C_i} z_{C_i} \\ I_{yz_i} &= I_{Cy'z'_i} + m_i x_{C_i} z_{C_i} \end{aligned} \tag{4.6}$$

where m_i is the mass of the section, $x_{C_i}, y_{C_i}, z_{C_i}$ are the distances from section centroid to the aircraft CG position calculated before and $I_{Cx'y'_i}, I_{Cx'z'_i}, I_{Cy'z'_i}$ are the cross moments of inertia around each of the sections centroid. Since all of the considered sections are

represented by symmetrical bodies, these can be said to be 0:

$$\begin{aligned} I_{Cx'y'_i} &= 0 \\ I_{Cx'z'_i} &= 0 \\ I_{Cy'z'_i} &= 0 \end{aligned} \quad (4.7)$$

Summing up the cross moments of all the sections, total cross moments of the aircraft are determined as:

$$\begin{aligned} I_{xy} &= \sum_{i=1}^n m_i x_{Ci} y_{Ci} \\ I_{xz} &= \sum_{i=1}^n m_i x_{Ci} z_{Ci} \\ I_{yz} &= \sum_{i=1}^n m_i y_{Ci} z_{Ci} \end{aligned} \quad (4.8)$$

where i is the number of each of different considered sections.

4.3. Results and Comparison

As stated in [1], during the flight test campaign, aircraft was weighted in accordance with the procedure described in POH [7]. Along with the weight of the aircraft, x_{CG} position was calculated from the moment of the weighted aircraft. Aircraft mass estimation provided exact values for the OEM and ATOM, comparing to the measured ones.

Table 4.1: Estimates comparison with weighting values

	Weighting	Estimates
OEM	751.67 kg	751.66 kg
ATOM	1008.08 kg	1008.2 kg
x_{CG} at OEM	2.2522 m	2.2531 m
x_{CG} at ATOM	2.251 m	2.2509 m

When estimating x_{CG} position using the *DATCOM* method and equations 4.5, results were off by somewhat 5 cm to the measured values. To get closer to the measured CG position values, x coordinates of six basic structural sections (representing OEM), that

were originally taken from the reconstructed CAD model, were reduced by 2%. This way, both OEM and ATOM x_{CG} position corresponded to the measured values and it was inside of the mass envelope. y_{CG} and z_{CG} position were not measured so there was no way to validate the estimates. That being said, x_{CG} position has much greater influence to the aircraft dynamics then the other two.

Table 4.2: CG position in ACS

	OEM [m]	ATOM [m]
x_{CG}	2.2531	2.2509
y_{CG}	0	-0.0032
z_{CG}	-0.07	-0.104

Since fuel is assumed to be equal along the y axis, it can be seen that y_{CG} is depending only on the crew mass and configuration. In the similar manner can be seen that cross moments of inertia having y component, are only dependent on the crew mass and configuration. That is why all the y components of the cross moments of inertia and y_{CG} are equal to 0 for OEM (no crew). This is because all of the other aircraft sections are symmetrical along the y axis, unlike the crew.

Table 4.3: Mass moments of inertia estimates in ACS

	OEM [kgm ²]	ATOM [kgm ²]
I_{xx}	1513.0	1890.3
I_{yy}	2082.1	2160.9
I_{zz}	3490.8	3861.6
I_{xy}	0	-5.4
I_{xz}	74.17	61.2
I_{yz}	0	2.2

All of the ATOM values, consider 34 USG of initial fuel and crew configuration with FTE sitting in front (forward CG).

5 Propulsion

With center of gravity position obtained , it is possible to get engine forces and moments needed for aerodynamic coefficients calculation. That is done using a Simulink engine model taken from the existing PA-28 model that was already implemented in the ReDSim. PA-28 engine model was first developed in [1] and implemented in ReDSim. Since model's implementation until the day of the start of this thesis, model has been slightly upgraded by other students at ZHAW.

MATLAB function *getEngData.m* as well as the standalone engine model *engine.slx* can be found in appendix B.2.

5.1. Engine Model

In the first iteration of the whole process, engine model was just taken out of the whole PA-28 ReDSim model and made as a standalone Simulink model. It had to be slightly modified and prepared for use with MATLAB script in a way of adding separate input and output signals (figure 5.1).

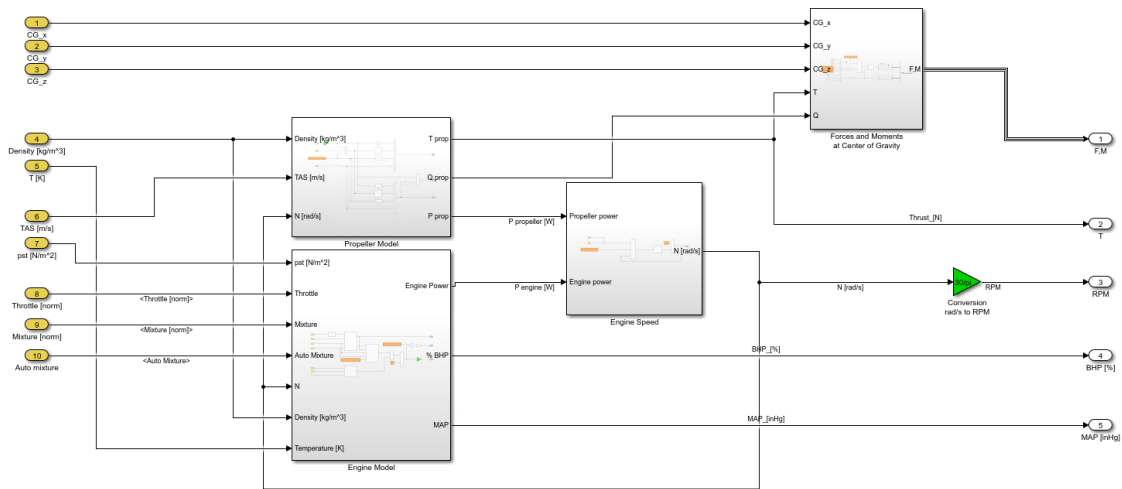


Figure 5.1: Standalone PA-28 Simulink engine model

Input signals come as values from the flight test data, such as temperature, altitude, air density, true airspeed, power setting etc. as well as calculated values of CG position. Since there was no record of the mixture lever position, mixture was always set to optimum mixture (FTE in [2] said that pilot was always trying to keep the mixture lever in the medium position). Due to the measurement error, throttle lever position was sometimes recorded over 100% or under 0%. This values were limited to 0-100%. Model also requires some constant values defined in the initialisation file of the whole PA-28 model (*iniac.m* file), such as atmospheric constants (gas constant, static density at 0km geopotential height...) and simulation constants (sample time or initial RPM). Output signals come as values for engine forces and moments, RPM, Brake horse power and manifold pressure.

It was later discovered that the engine model does not provide correct output compared to the actual flight test data. That can best be seen looking at the RPM. Figure 5.2 shows RPM for two short period manoeuvres, followed by stall and a phugoid manoeuvre.

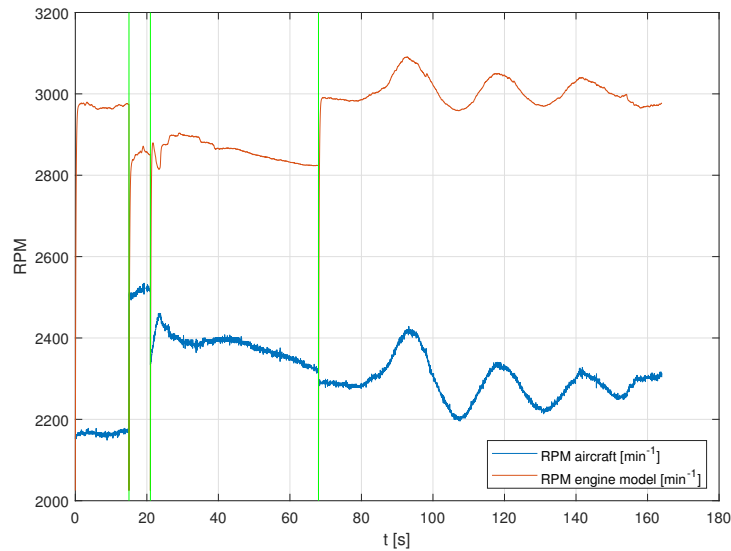


Figure 5.2: RPM of the older version of the engine model RPM compared to the measured RPM

It can be seen that model values greatly differ from actual RPM values. Because of that, in order to match the actual output of the engine, it was decided to do the mapping of the power setting i.e. throttle lever position to the power setting that would provide the correct output.

5.2. Throttle Mapping

Throttle mapping was not done in the course of this thesis. It was rather done by other students at ZAV, working on the same PA-28 project. Main goal is to match the output model values to the measured ones. Since only measured engine parameter is the engine RPM, mapping was done comparing the RPM of the model with the recorded RPM. Basically, it is developing a function that corrects recorded throttle position to the value that, put in the model, provides an output RPM as close to the recorded one. Figure 5.3 presents a basic scheme of the process.

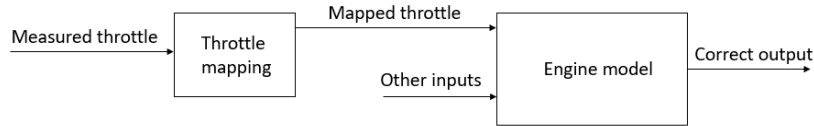


Figure 5.3: Mapping process of the power setting

After mapping the power setting and correcting some other mistakes in the engine model, output provided by the model improved significantly. Figure 5.4 shows the same manoeuvres but with simulated RPM much closer to the actual RPM.

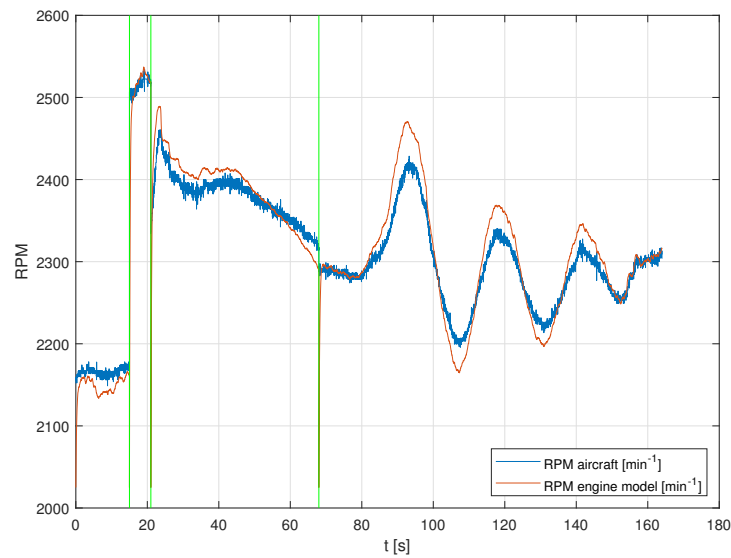


Figure 5.4: Engine model RPM with throttle mapping compared to the measured RPM

With so verified and corrected engine model, it was decided to proceed with the project considering engine forces and moments provided by the model.

5.2.1. Engine Model Initialization

Another problem that had to be dealt with is the initialization of the engine model. In the previous figures 5.4 and 5.2 as well as closer look in the figure 5.5 it can be seen that, in the beginning of every manoeuvre, there is a transient period where RPM goes from the initial value to the actual value defined by the data. That is because the engine model needs some time to settle on the actual value from the initial RPM that is set as a constant in the initialisation file. This can introduce some irregularities later in the aerodynamic coefficient calculation.

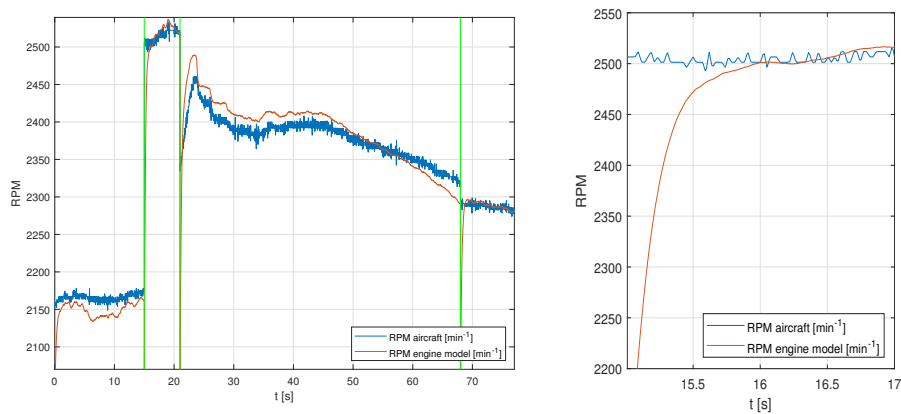


Figure 5.5: Closer view of the engine model transient behaviour

In order to get rid of the transients, model is initialized with introducing a period of few seconds before the start of the actual manoeuvre. Input parameters, in the initialisation period, are the same as the first point of the flight test data at the start of each manoeuvre. This way engine model is running on a simulated set of data, equal to the first actual data point, until it overcomes the period of the transient behaviour. Later, when accessing the output parameters, this period of initialisation is just removed from the data leaving the starting point of the manoeuvre data as it was, but with exact value. This can be seen on figure 5.6, where the transient behaviour of the engine model RPM is not present any more.

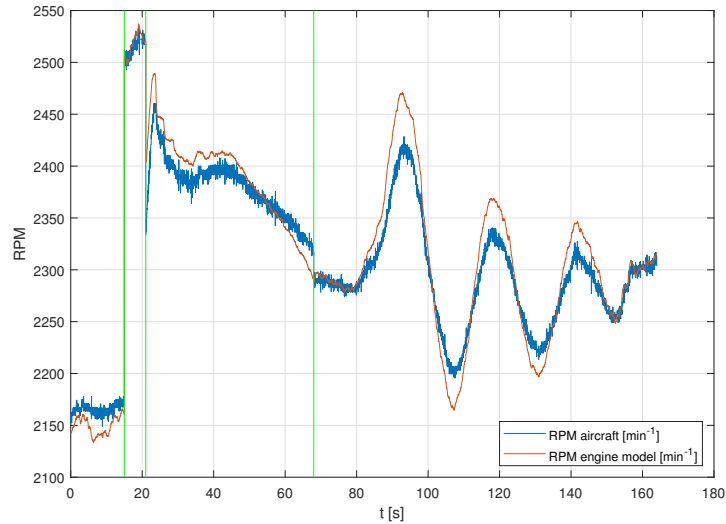


Figure 5.6: Final engine model response with initialisation of the engine implemented

5.3. Engine Forces and Moments

Running the engine model for just one instance of the certain test point (short period manoeuvre), engine forces and moments come as:

Table 5.1: Example of the engine forces and moments in BCS for an instance of a short period manoeuvre

Parameter	Value
X_e	≈ 950 N
Y_e	0 N
Z_e	0 N
L_e	≈ -230 Nm
M_e	≈ -100 Nm
N_e	≈ -3 Nm

It is important to mention that the engine model expects the CG coordinates to be defined in ACS while the forces and moments come as output elements in BCS.

6 | Data Corrections

In this chapter, it is shown how flight test data is corrected for some errors mentioned in section 2.1.3., as well as some additional errors discovered later when working with the FTD. Also necessary measurement noise filtering is described along with calculation of additional parameters needed in parameter estimation.

Readers who would like to use MATLAB and other utilities for data correction are referred to appendix B.3.

6.1. Data Correction for IMU Installation Angle

Already in previous master thesis [2], during the FPR, it was discovered that there is an IMU installation angle that misaligns the IMU coordinates from the body coordinates (figure 6.2). That was introducing great inconsistency to the IMU data, compared to the cRIO data. Axes of the cRIO measurement unit (and all the data collected by cRIO) are aligned with the body coordinates. Axes of the IMU should also be aligned with the body coordinates in order to be precisely coherent with the rest of the data. That being said, installation angle of the IMU i.e. the angle of the baggage compartment floor was needed. To solve that issue, visit¹ to the hangar of the PA-28 aircraft was organised. Aircraft was the same PA-28 aircraft but not the actual test aircraft that was used in flight test campaign. The angle of the baggage compartment floor, relative to the body coordinates, was measured using a digital spirit level (figure 6.1).

¹During this visit, some coordinates of the IMU and the ADB were measured (appendix C.1.)



Figure 6.1: Measuring the water line level of the aircraft

Level was placed on the bolts below the front window, following the procedure from the AMM [6], marking the water line level of the aircraft.

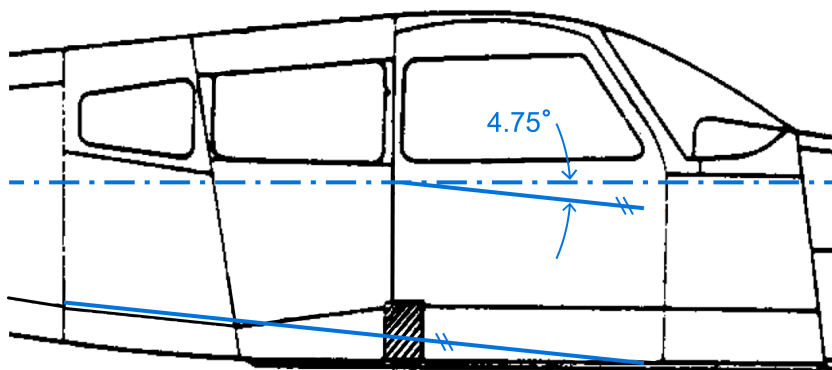


Figure 6.2: Baggage floor (IMU installation angle) angle with reference to the aircraft's water line

The angle of the baggage compartment was measured to be $\alpha_{IMU} = 4.75^\circ$.

After that, accelerations and rotational rates of the aircraft, coming from the IMU, are easily transformed to the body coordinates using the rotational matrix [13]:

$$\mathbf{L}_y = \begin{bmatrix} \cos \alpha_{IMU} & 0 & -\sin \alpha_{IMU} \\ 0 & 1 & 0 \\ \sin \alpha_{IMU} & 0 & \cos \alpha_{IMU} \end{bmatrix} \quad (6.1)$$

Rotational rates are simply corrected:

$$\begin{bmatrix} p_b \\ q_b \\ r_b \end{bmatrix} = \begin{bmatrix} \cos \alpha_{IMU} & 0 & -\sin \alpha_{IMU} \\ 0 & 1 & 0 \\ \sin \alpha_{IMU} & 0 & \cos \alpha_{IMU} \end{bmatrix} \begin{bmatrix} p \\ q \\ r \end{bmatrix} \quad (6.2)$$

where $[p_b, q_b, r_b]$ are the rotational rates in body coordinate system and the alpha is the measured angle in radians. Linear accelerations are corrected in the same way. Correction of rotational rates and linear accelerations for IMU installation angle can be seen on figure 6.3 for one short period manoeuvre.

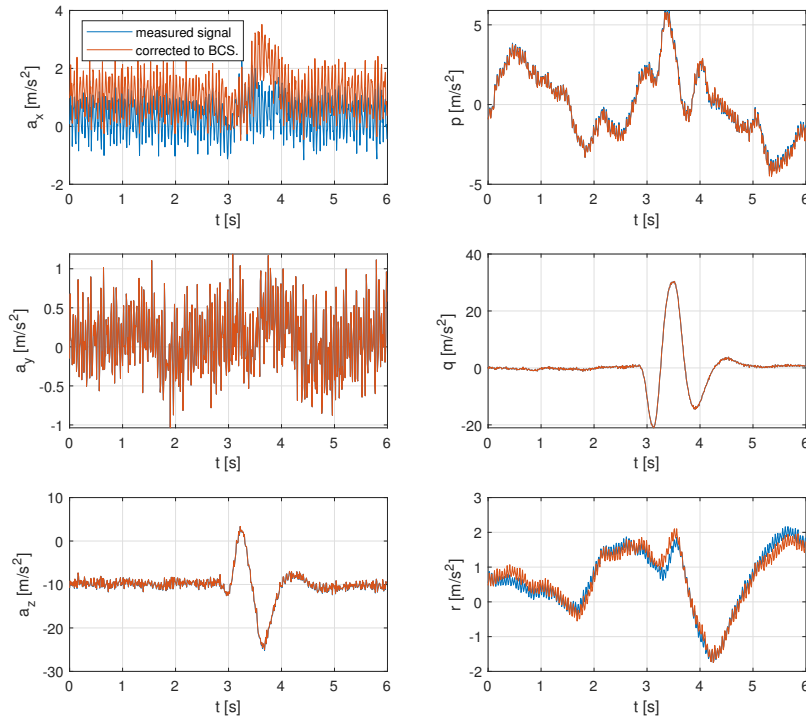


Figure 6.3: Correction of rotational rates and linear accelerations for misalignment angle $\alpha_{IMU} = 4.75^\circ$ for a short period manoeuvre

It can be seen that y axis values did not change since the rotation is only made around y axis.

Pitch angle also had to be corrected by misalignment angle in a way that the angle is just added as an offset to the pitch angle:

$$\theta_b = \theta + 4.75^\circ \quad (6.3)$$

where θ_b is the pitch angle in body coordinate system.

Now, the IMU and the cRIO (ADB) data is mutually consistent and it can be further corrected and analysed.

6.2. Filtering FTD Parameters

Another necessary step in FTD correction is filtering signals for measurement noise reduction. Measurement instrumentation and sensors are not perfect and often record data with some amount of noise. When dealing with signals and parameters that follow dynamic motion of the aircraft, measurement noise can make the signals hard to read or, with high noise, even cover the dynamics. Also, using unfiltered data in calculations introduces even higher noise to the output variables which can seriously aggravate data analysis like for example regression in parameter estimation. That is why certain parameters are filtered with so called low pass filters removing the higher frequency noise. Filter used in this thesis is a first-order zero-phase discrete time filter developed at ZAV during a past project [4] and available as *lowPassFilter.m* in appendix B.3.

Most important is to properly filter rotational rates since they have an effect in all further calculations. For example, derivatives of the rotational rates (equation 6.5) are the biggest problem, since deriving can amplify the noise to the point that graphs become completely unreadable.

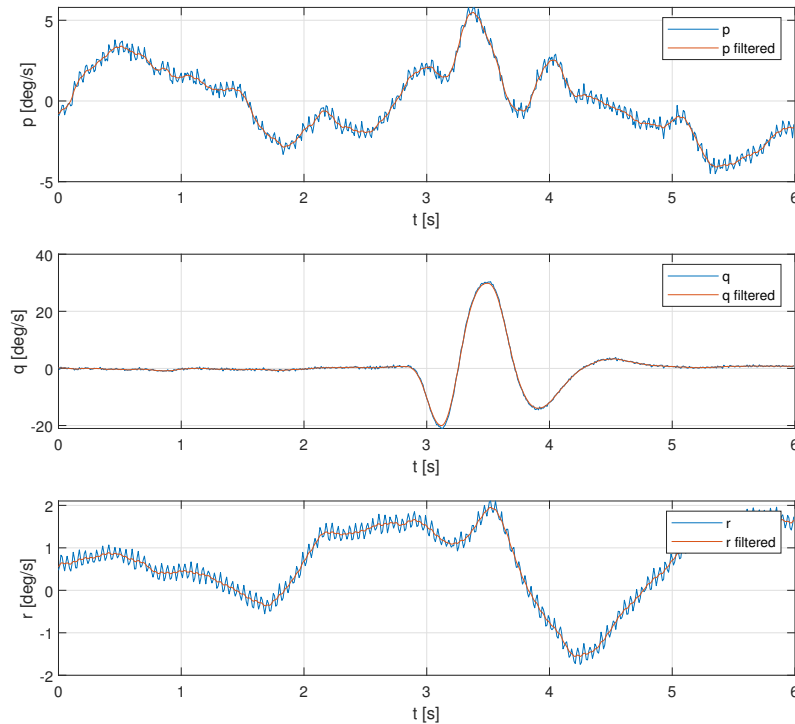


Figure 6.4: Measured and filtered rotational rates p, q, r for a short period manoeuvre

Figure (6.4) shows the unfiltered and filtered rotational rates for a short period manoeuvre. The cut-off frequency is set in such a way that only frequencies higher than the defined one are filtered. Meaning that just the higher frequency noise is filtered out, but the relevant dynamics of the signal remains unchanged (i.e. the dynamics of the aircraft at lower frequencies).

The same low-pass filter is applied to the measured and corrected for off-CG position accelerations, but with a different cut-off frequency. The reason for this is simply to remove some of the higher frequency noise on the measured signal as the measured linear accelerations come with a higher noise than rotational rates. Figure 6.5 shows filtering of the linear accelerations for the same short period manoeuvre.

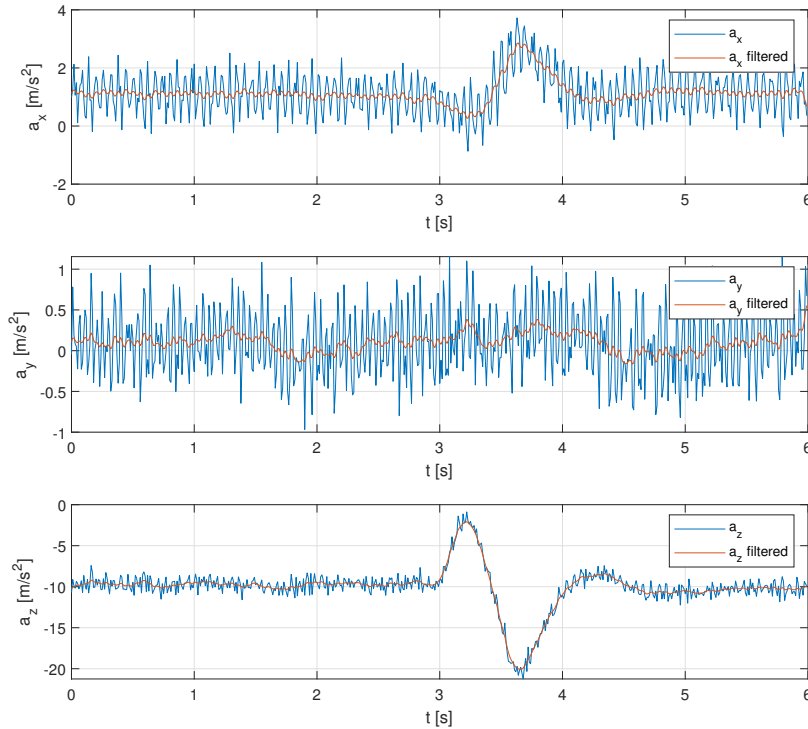


Figure 6.5: Measured and filtered linear accelerations a_x, a_y, a_z for a short period manoeuvre

Other parameters, can also be filtered as needed but one should take good care as filters like this, if not being careful, can easily kill the dynamics of the measured signal. Usually, filtering is done only when absolutely necessary by applying the filter only to the noisy signals that would otherwise, further in calculations, introduce higher noise or make the dynamics unreadable. In this work, only the rotational rates are filtered before their usage in any calculation. Even though accelerations are shown to be filtered in this section, they are used in the filtered form only when completely needed.

The cut-off frequencies ω_c for the filter are:

- $p, q, r \ \omega_c = 50 \text{ rad s}^{-1}$
- $a_x, a_y, a_z \ \omega_c = 40 \text{ rad s}^{-1}$

6.3. Off-CG Corrections

Next step is to correct aircraft's linear accelerations for the off-CG position. Accelerations are measured by the IMU which is placed in the baggage compartment that does not coincide with the aircraft's CG position. Linear accelerations are supposed to be defined for the CG position so it is necessary to correct them. Since IMU's axis are now aligned with the body axis coordinate frame, the accelerations at the CG can be calculated from the measured accelerations as [3]:

$$\begin{aligned}
 a_x &= a_x^{IMU} + (q^2 + r^2)x_{IMU,CG} - (pq - \dot{r})y_{IMU,CG} - (pr + \dot{q})z_{IMU,CG} \\
 a_y &= a_y^{IMU} - (pq + \dot{r})x_{IMU,CG} + (p^2 + r^2)y_{IMU,CG} - (qr - \dot{p})z_{IMU,CG} \\
 a_z &= a_z^{IMU} - (pr - \dot{q})x_{IMU,CG} - (qr + \dot{p})y_{IMU,CG} + (p^2 + q^2)z_{IMU,CG}
 \end{aligned} \tag{6.4}$$

where $[a_x, a_y, a_z]$ and $[a_x^{IMU}, a_y^{IMU}, a_z^{IMU}]$ are the accelerations at the CG and the IMU position, respectively. The position of the IMU with respect to the CG in body axis coordinates is $[x_{IMU,CG}, y_{IMU,CG}, z_{IMU,CG}]$. $[p, q, r]$ are the filtered (section 6.2.) rotational rates. Note also that the rotational accelerations $[\dot{p}, \dot{q}, \dot{r}]$ are not measured directly but are obtained by numerical differentiation of the measured angular rates [3].

$$\begin{aligned}
 \dot{p} &= \Delta p / \Delta t \\
 \dot{q} &= \Delta q / \Delta t \\
 \dot{r} &= \Delta r / \Delta t
 \end{aligned} \tag{6.5}$$

When calculating the distance from the IMU to the CG, x and z values should be multiplied by -1 since the IMU and CG coordinates are specified in ACS while the offset, like all the other relevant data, should be in BCS:

$$\begin{aligned}
 x_{IMU,CG} &= -1(x_{IMU} - x_{CG}) \\
 y_{IMU,CG} &= y_{IMU} - y_{CG} \\
 z_{IMU,CG} &= -1(z_{IMU} - z_{CG})
 \end{aligned} \tag{6.6}$$

ADB offsets are calculated using the same equations. IMU coordinates in ACS are stated in section 3.2. while ADB coordinates in ACS are defined in section 6.4.1. The same conversion matrix is used in section 7. for converting moments of inertia and CG

position from ACS to BCS:

$$\mathbf{A2B} = \begin{bmatrix} -1 & 0 & 0 \\ 0 & 1 & 0 \\ 0 & 0 & -1 \end{bmatrix} \quad (6.7)$$

6.4. Correcting Air Data

As stated in section 2.1.3., there are measurement errors that affect the accuracy of the flight test data. Specifically, the ADB errors. These are, as previously (section 2.1.3. and 3.3.4.) explained, the error because of the airflow around the ADB itself, the error because of the airflow around the aircraft (position error) and a pressure lag. They all have an effect on the AoS, AoA, static and dynamic pressure and they all have to be resolved/reduced. The error because of the airflow around the ADB itself is already corrected, in [2], using a sensor error model developed with calibration of the ADB in the wind tunnel. Another common way of building sensor error models is a flight path reconstruction.

6.4.1. Air Data Boom

Air Data Boom (figure 6.6) is a measurement unit which has an integrated pitot-static tube measuring the total p_{total} and static p_s pressure. The (local) flow angles AoA α and AoS β are both measured with potentiometers integrated in the ADB as well.

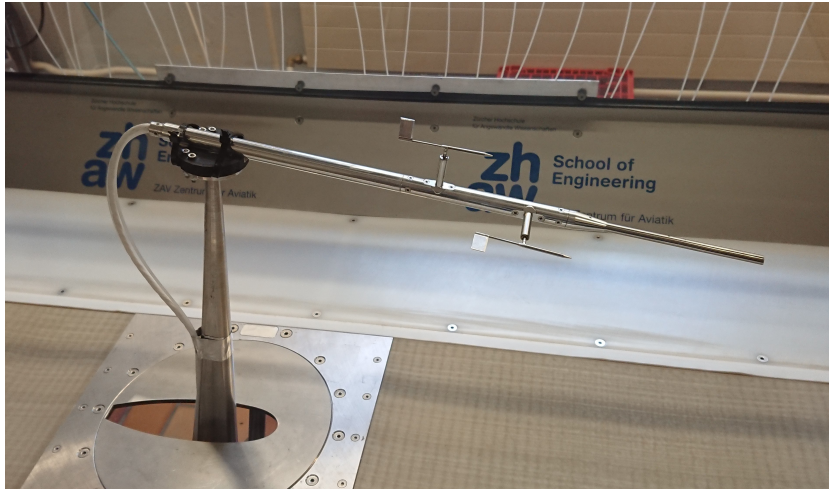


Figure 6.6: Air Data Boom (ADB) measurement unit [2]

The ADB is mounted at the end of the right wing, at the level of the aircraft's center line (x axis in body frame). For greater reduction of the airflow errors, it is mounted, using an extender rod, approximately one wing tip chord ahead of the wing leading edge. This way, coordinate axes of the ADB are aligned with the body axes of the aircraft. Detailed description and installation methods can be seen in [2] and [1]. The coordinates of the ADB in ACS are:

$$x_{ADB} = 1.17 \text{ m}$$

$$y_{ADB} = 5.32 \text{ m}$$

$$z_{ADB} = 0 \text{ m}$$

Way of obtaining the ADB coordinates is described in appendix C.1.

6.4.2. Flight Path Reconstruction

The Flight Path Reconstruction (FPR), also known as data compatibility check, is a procedure to reconstruct the trajectory of an aircraft. Combining measurements from the flight tests with the kinematic equations allows the reconstruction of states that are not directly observed. If measurements of different parameters are combined, the FPR can also be used to estimate sensor errors.

Kinematic equations provide, as shown in [3] a way to reconstruct the states during flight testing. From these states other signals that are measured during flight testing

can be calculated, such as the true airspeed or dynamic pressure, the AoA and the AoS. Since these parameters were measured in flight, the compatibility of the two different sources of data can be checked. If the data shows systematic discrepancies, a sensor error model can be constructed and estimated.

FPR, as well as some basic sensor error models, for the flight test data obtained during the flight test campaign, was already done in [2]. However, it was discovered, in the course of this thesis, that the FPR done in the preceding thesis did not take into account the installation angle (section 6.1.) of the IMU correctly. That is why it was decided to reconstruct the basic sensor error models for the quantities measured by the ADB i.e. dynamic pressure, the AoA and the AoS. Due to the limited time, sensor error models were developed to the satisfactory but not perfect level and there is still space for improvements.

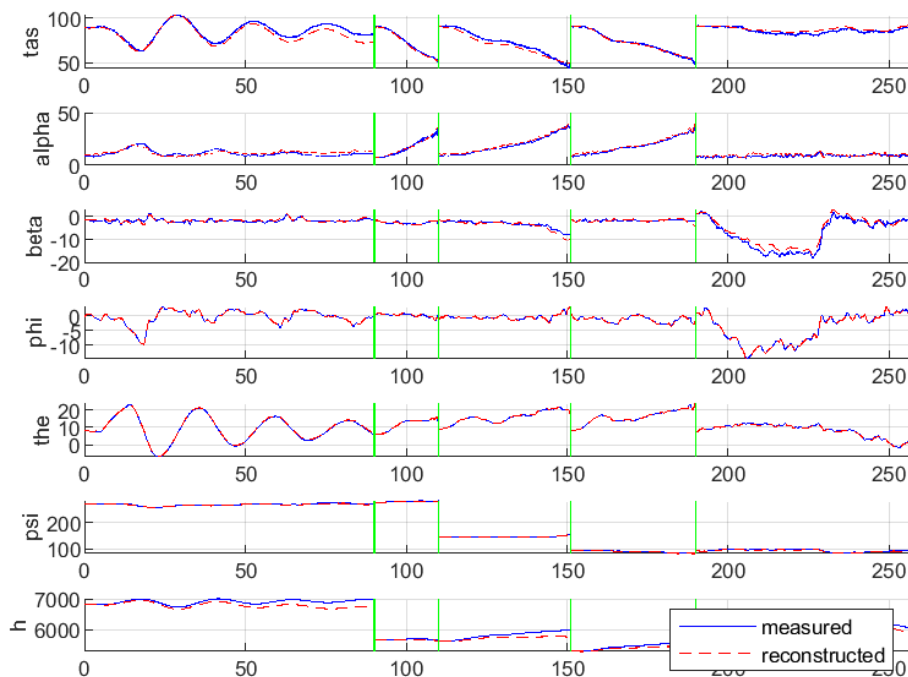


Figure 6.7: FPR results for a phugoid, three stall manoeuvres and a steady heading steady sideslip manoeuvre

Results of the FPR can be seen on figure (6.7) for manoeuvres with lower dynamic response, such as phugoid, stall and steady heading steady sideslip manoeuvre. As the measured values of these manoeuvres follow the reconstructed ones quite closely, it can be said that used sensor error models correct measured data on a quite satisfactory level. Still, when dealing with manoeuvres with higher dynamic response, match between measured and reconstructed quantities is not so close. Figure (6.8) presents the results of the FPR for three short period manoeuvres and two dutch roll manoeuvres.

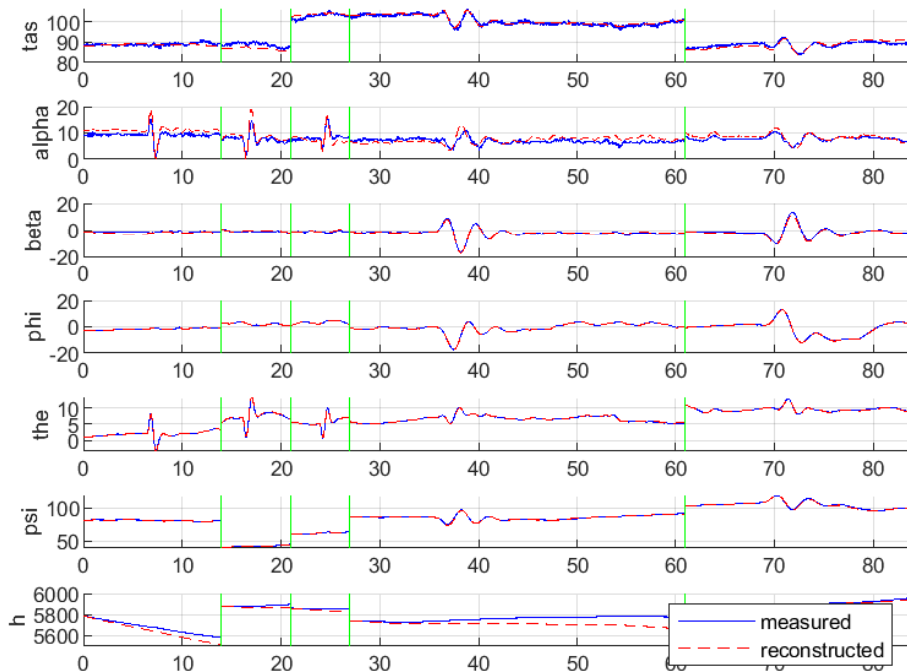


Figure 6.8: FPR results for three short period manoeuvres and 2 dutch rolls

Looking at the AoA and the AoS it can be seen that the measured signals does not follow the dynamics of the reconstructed signals as close as the ones on the previous figure (6.7). That being said, for the purposes of this work, sensor error models that provided these results were chosen for correcting measured parameters. These models are presented as it follows:

- Angle of attack α_{corr} :

$$\alpha_{corr} = (\alpha_m - b_\alpha)/k_\alpha \quad (6.8)$$

where:

$$b_\alpha = -0.1$$

$$k_\alpha = 1.8$$

- Angle of sideslip β_{corr} :

$$\beta_{corr} = (\beta_m - b_\beta)/k_\beta \quad (6.9)$$

where:

$$b_\beta = 0$$

$$k_\beta = 1$$

- Dynamic pressure q_{corr}

$$q_{corr} = (q_{cm} - b_{qc})/k_q \quad (6.10)$$

with:

$$b_{qc} = -150$$

$$k_{qc} = 1.1$$

where measure dynamic pressure q_{cm} is calculated from measured static pressure p_s and using *TAS* (equation 3.3) with:

$$\begin{aligned} M &= TAS/a \\ q_{cm} &= p_s((1 + 0.2 \cdot M^2)^{(7/2)} - 1) \end{aligned} \quad (6.11)$$

a being the local speed of sound in air calculated:

$$a = \sqrt{\gamma \cdot R \cdot T} \quad (6.12)$$

with $\gamma = 1.4$ being air heat capacity ratio, T local temperature and R specific air gas constant (equation 3.2). Corrected true airspeed TAS_{corr} is then calculated back from corrected dynamic pressure:

$$\begin{aligned} M_{corr} &= \sqrt{5(((q_{corr}/p_s) + 1)^{(2/7)} - 1)} \\ TAS_{corr} &= M_{corr} \cdot a \end{aligned} \quad (6.13)$$

It is necessary to say that shown models are actually inverse models of the ones developed with FPR. In the FPR, as it is set up for the purpose of this work, reconstructed data is actually corrected to fit the measured data. Since it is necessary to correct the measured parameters to the reconstructed ones, hence the inversion. Also, important to mention is that the models expect the angles (AoA,AoS) to be in radians.

Figure 6.9 shows an example of air data correction with the upper error models for one short period and one stall manoeuvre.

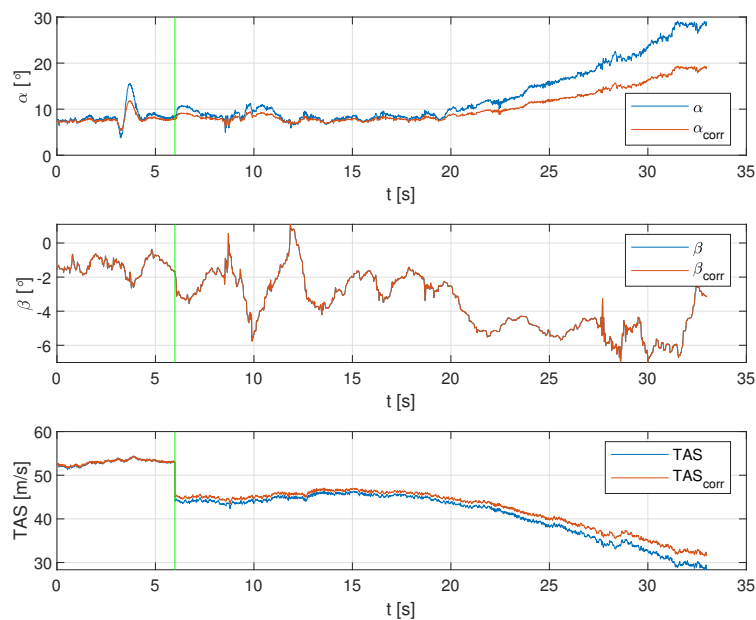


Figure 6.9: Sensor error model corrections to air data for one short period manoeuvre and one stall manoeuvre

All utilities needed for the FPR can be found in appendix B.5.

6.4.3. Correcting Air Data for off-CG Position

After applying sensor error models, developed with FPR, to the measured air data, data is corrected for the off-CG position like the accelerations before. Computation of the AoA, AoS and true airspeed at the CG is done following the equations from the

[14] and [3]. First, the body axis velocity components at the ADB position have to be calculated from the corrected (section 6.4.2.) measured signals with:

$$\begin{aligned} u^{ADB} &= TAS^{ADB} \cos \alpha^{ADB} \cos \beta^{ADB} \\ v^{ADB} &= TAS^{ADB} \sin \beta^{ADB} \\ w^{ADB} &= TAS^{ADB} \sin \alpha^{ADB} \cos \beta^{ADB} \end{aligned} \quad (6.14)$$

where the superscript ADB denotes the ADB position. Secondly, the velocity components at the CG can be calculated as:

$$\begin{aligned} u^{CG} &= u^{ADB} + r \cdot y_{ADB,CG} - q \cdot z_{ADB,CG} \\ v^{CG} &= v^{ADB} + p \cdot z_{ADB,CG} - r \cdot x_{ADB,CG} \\ w^{CG} &= w^{ADB} + q \cdot x_{ADB,CG} - p \cdot y_{ADB,CG} \end{aligned} \quad (6.15)$$

where $[x_{ADB,CG}, y_{ADB,CG}, z_{ADB,CG}]$ is the distance of the ADB relative to the CG, calculated in the same manner (equation 6.6) as the IMU offset in section 6.3. Finally, true airspeed, the AoA, and the AoS at the CG can be calculated by:

$$\begin{aligned} TAS_{CG} &= \sqrt{(u^{CG})^2 + (v^{CG})^2 + (w^{CG})^2} \\ \alpha_{CG} &= \tan^{-1}(w^{CG}/u^{CG}) \\ \beta_{CG} &= \sin^{-1}(v^{CG}/TAS_{CG}) \end{aligned} \quad (6.16)$$

After obtaining true airspeed at the CG position, it is possible to calculate normalized rotational rates which are needed later in section 8.:

$$\begin{aligned} p^* &= p \cdot b / (2TAS_{CG}) \\ q^* &= q \cdot \bar{c} / (2TAS_{CG}) \\ r^* &= r \cdot b / (2TAS_{CG}) \end{aligned} \quad (6.17)$$

where b is the aircraft wingspan and \bar{c} is the mean aerodynamic chord both specified in section 3.1.

Figure 6.10 shows the off-CG position correction of the air data for one short period and one dutch roll manoeuvre.

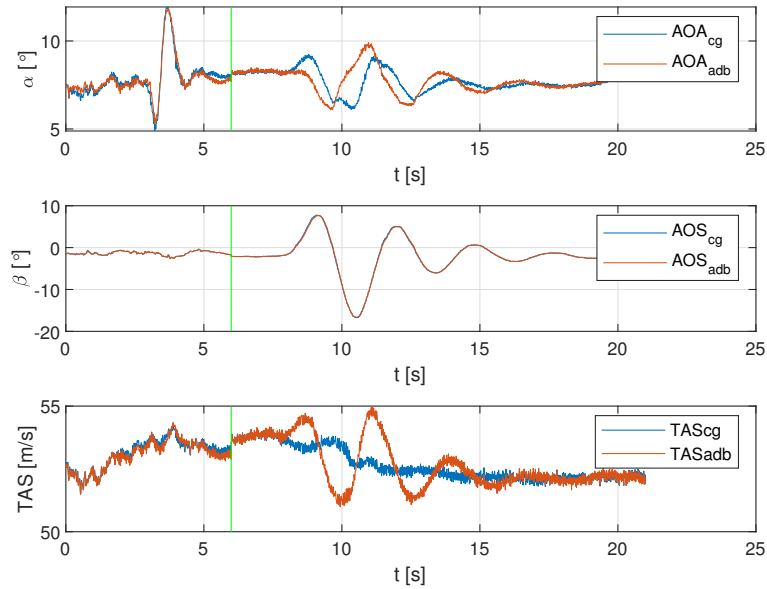


Figure 6.10: Off-CG air data correction for a short period and a dutch roll manoeuvre

It can be seen that the values of the AoA, AoS and true airspeed for a short period manoeuvre do not significantly differ from the corrected values. That is because the short period manoeuvre is performed with relatively small change considering the aircraft movement across the lateral axis. On the other hand, corrected AoA and true airspeed for a dutch roll manoeuvre have significantly different values from the off-CG values. Due to the aircraft motion, the airflow at the CG is different from the one at the wing tip (ADB position) so for the manoeuvres with lateral dynamics correction will be greater.

7 Aerodynamic Coefficients

Even though the total aerodynamic coefficients can not be directly measured, it is quite simple to compute them. The equations in this section can be obtained from the equations of motion in body axis frame. These equations can also be found in [13], [3].

Under the assumption that the aircraft is a point mass, the resultant aerodynamic forces and moments act at the CG. To calculate the aerodynamic forces and moments it is sufficient to measure the linear accelerations and the rotational rates at the CG. If the linear accelerations are measured at an off-CG position, they can be easily transformed to the CG like it is shown in section 6.3. The aerodynamic forces at the CG in body axis can then be calculated by

$$\mathbf{F}_{aero} = m\mathbf{a} - \mathbf{F}_{eng} = \begin{bmatrix} F_{x,aero} \\ F_{y,aero} \\ F_{z,aero} \end{bmatrix} = m \begin{bmatrix} a_x \\ a_y \\ a_z \end{bmatrix} - \begin{bmatrix} X_e \\ Y_e \\ Z_e \end{bmatrix} \quad (7.1)$$

where \mathbf{F}_{eng} is the force vector from the engine. The aerodynamic coefficients in body axes can then be calculated by

$$\begin{bmatrix} C_x \\ C_y \\ C_z \end{bmatrix} = \frac{1}{qS} \mathbf{F}_{aero} \quad (7.2)$$

where q is the dynamic pressure and S is the wing reference area. Usually, one is more interested in the lift, drag and sideforce coefficients. These can be calculated from the

body axes coefficients by

$$\begin{bmatrix} C_D \\ C_y \\ C_L \end{bmatrix} = \begin{bmatrix} \cos \alpha & 0 & \sin \alpha \\ 0 & 1 & 0 \\ -\sin \alpha & 0 & \cos \alpha \end{bmatrix} \begin{bmatrix} -C_x \\ C_y \\ -C_z \end{bmatrix} \quad (7.3)$$

where α is the angle of attack. The aerodynamic moment coefficients can be calculated in a similar manner. The aerodynamic moments at the CG are:

$$\begin{aligned} \mathbf{M}_{aero}^{CG} &= \mathbf{I}\dot{\boldsymbol{\Omega}} + \boldsymbol{\Omega} \times (\mathbf{I}\boldsymbol{\Omega}) - \mathbf{M}_{eng} = \\ \begin{bmatrix} L \\ M \\ N \end{bmatrix} &= \begin{bmatrix} I_{xx} & -I_{xy} & -I_{xz} \\ -I_{xy} & I_{yy} & -I_{yz} \\ -I_{xz} & -I_{yz} & I_{zz} \end{bmatrix} \begin{bmatrix} \dot{p} \\ \dot{q} \\ \dot{r} \end{bmatrix} + \begin{bmatrix} p \\ q \\ r \end{bmatrix} \\ &\times \left(\begin{bmatrix} I_{xx} & -I_{xy} & -I_{xz} \\ -I_{xy} & I_{yy} & -I_{yz} \\ -I_{xz} & -I_{yz} & I_{zz} \end{bmatrix} \begin{bmatrix} p \\ q \\ r \end{bmatrix} \right) - \begin{bmatrix} L_e \\ M_e \\ N_e \end{bmatrix} \end{aligned} \quad (7.4)$$

where \mathbf{I} is the inertia tensor, $\boldsymbol{\Omega}$ is the vector of the rotational rates at the CG, $\dot{\boldsymbol{\Omega}}$ is the vector for the rotational accelerations and \mathbf{M}_{eng} are the moments from the engine at the CG. It is usually more convenient to work with moment coefficients that refer to the aerodynamic reference point than to the CG. That is why they are converted to the moments at the aerodynamic reference point (indicated with the superscript RP) by:

$$\begin{aligned} \mathbf{M}^{RP} &= \mathbf{M}^{CG} - \mathbf{F}_{aero} \times \mathbf{D}_{RPCG} \\ \begin{bmatrix} L \\ M \\ N \end{bmatrix}^{RP} &= \begin{bmatrix} L \\ M \\ N \end{bmatrix}^{CG} - \begin{bmatrix} F_{x,aero} \\ F_{y,aero} \\ F_{z,aero} \end{bmatrix} \times \begin{bmatrix} x_{RPCG} \\ y_{RPCG} \\ z_{RPCG} \end{bmatrix} \end{aligned} \quad (7.5)$$

where the vector \mathbf{D}_{RPCG} is the distance between the aerodynamic reference point and the CG with reference point coordinates in ACS being:

$$\begin{aligned} x_{RP} &= 2.3919 \text{ m} \\ y_{RP} &= 0 \text{ m} \\ z_{RP} &= -0.1524 \text{ m} \end{aligned}$$

Finally, the aerodynamic moment coefficients can be calculated by:

$$\begin{bmatrix} C_l \\ C_m \\ C_n \end{bmatrix}^{RP} = \frac{1}{qS} \begin{bmatrix} 1/b & 0 & 0 \\ 0 & 1/\bar{c} & 0 \\ 0 & 0 & 1/b \end{bmatrix} \begin{bmatrix} L \\ M \\ N \end{bmatrix}^{RP} \quad (7.6)$$

where b is the wing span and \bar{c} is the mean aerodynamic chord.

Also, thrust coefficient is calculated with:

$$C_T = X_e / (q_c \cdot S_{Ref}) \quad (7.7)$$

With the thrust and aerodynamic coefficients defined, all the necessary quantities are gathered and everything is ready for the parameter estimation, described in the following section.

Aerodynamic and thrust coefficients are all calculated with the script *getAeroCoeff.m* available in appendix [B.3.](#)

8 Parameter Estimation With Linear Regression

With all the coefficients determined, next step is the parameter estimation. Parameter estimation, regarding aerodynamic coefficients, is a process of obtaining models (for aerodynamic coefficients computation) and it's parameters which closely follow actual aerodynamic coefficients, computed from the measured data (section 7.). Many different model postulates can be explored. A common choice for the representation of the aerodynamic model developed from flight test data is the form of polynomials. For example, the lift coefficient could be represented as:

$$C_L = C_{L,0} + C_{L,\alpha} \cdot \alpha + C_{L,\alpha^2} \cdot \alpha^2 + C_{L,\alpha\beta} \cdot \alpha \cdot \beta \quad (8.1)$$

As it is easier to fit linear than non-linear models, for the purposes of this thesis, polynomials are not considered and all the models were set to be represented with a basic linear regression. In linear regression the relationships are modelled using linear predictor functions whose unknown model parameters are estimated from the data:

$$C_m = C_{m_0} + f_1(\alpha) + f_2(\delta_e) + f_3(C_T) + f_4(q^*) + f_5(\alpha, C_T) \quad (8.2)$$

To fit the models to the actual values, as it is often a practice, estimation is done with ordinary least squares method. The method is based on minimizing the sum of the squares of the residuals, with residuals being the difference between an observed value and the fitted value provided by the model. In other words, fitting is done in order for the difference between the measured and modelled signal to be as small as possible, for every data point.

8.1. Introduction to modelling

When constructing different models for aerodynamic coefficients, the same principle should always be followed. Models should be as simple as possible but still represent certain dynamics in the best way. Also, special care should be taken when choosing the manoeuvres which are best suitable for each of the coefficients and which are best representing the desired dynamics. For example, if the analysed model is the model for the pitching moment coefficient, manoeuvres exciting the greatest change in AoA or the pitch rate are the one to be chosen. This way, most influence of the AOA and pitch rate derivatives will be included in the model.

Another thing, with least squares method and the function used in this thesis is that there is a weight factor that gives more weight to the test points having longer duration. That being said, stall manoeuvres can have a duration from 20 to 70 seconds while the short manoeuvres usually take 6 seconds. If they are used in the same estimation, function will give more weight to the stall manoeuvre. This is solved in a way that the duration of all the longer manoeuvres (stall, phugoid etc.) is met with more of the shorter manoeuvres (short period). This way, different manoeuvres are given approximately equal weight, which can best be seen in figure 8.1.

Ideally all test points and the whole flight envelope should be fitted with the same aerodynamic coefficient models. Since in the process of modelling, that is not always possible, it is important to follow which test points and manoeuvres are covered by the models and what are their features. Different manoeuvres are performed with different configurations and they all have an effect on the aircraft dynamics which can be modelled with different parameters.

It is important to mention that all developed models are valid only in the scope of their own limits and in the scope of the manoeuvres and parameters they were developed with. For example, models that does not incorporate AoS and are not developed with respect to the manoeuvres with high changes in AoS, can not be expected to provide satisfactory results for conditions with high variations in AoS present.

For the models developed in the next sections, by no means do they represent exact and absolutely correct models but are rather ones that are brought to the satisfactory level required from this thesis. They can all be significantly improved in the way of following the specified dynamics completely and covering the whole flight envelope in total.

All the estimation scripts and functions can be found in appendix B.4.

8.2. Base models

As a starting point for all the coefficient estimations, basic exemplary models from [3] were chosen:

$$\begin{aligned}
 C_D &= C_{D0} + C_{D\alpha}\alpha \\
 C_L &= C_{L0} + C_{L\alpha}\alpha \\
 C_m &= C_{m0} + C_{m\alpha}\alpha + C_{mq}q^* + C_{m\delta_e}\delta_e \\
 C_Y &= C_{Y0} + C_{Y\beta}\beta \\
 C_l &= C_{l0} + C_{l\beta}\beta + C_{lp}p^* + C_{lr}r^* + C_{l\delta_a}\delta_a \\
 C_n &= C_{n0} + C_{n\beta}\beta + C_{np}p^* + C_{nr}r^* + C_{n\delta_r}\delta_r
 \end{aligned} \tag{8.3}$$

After that, estimation was divided in two segments, first one being the longitudinal and second the lateral motion coefficients. Models were gradually upgraded and the regression was providing better results with each iteration. Also, more of the manoeuvres were covered by the same models, considering different test flights and configurations.

8.3. Longitudinal motion coefficients

Longitudinal motion was chosen to be dealt with first. Due to limited time, aerodynamic coefficient models of this segment were explored with more attention and commitment. For simplicity reasons, it was decided to start with the pitch moment coefficient C_m model, followed by lift coefficient C_L and drag coefficient C_D model.

8.3.1. Pitching moment coefficient model

For pitching moment coefficient, it was decided to estimate the parameters looking at the short period and stall manoeuvres. After introducing the base model, results of the estimation were generally good (figure 8.1).

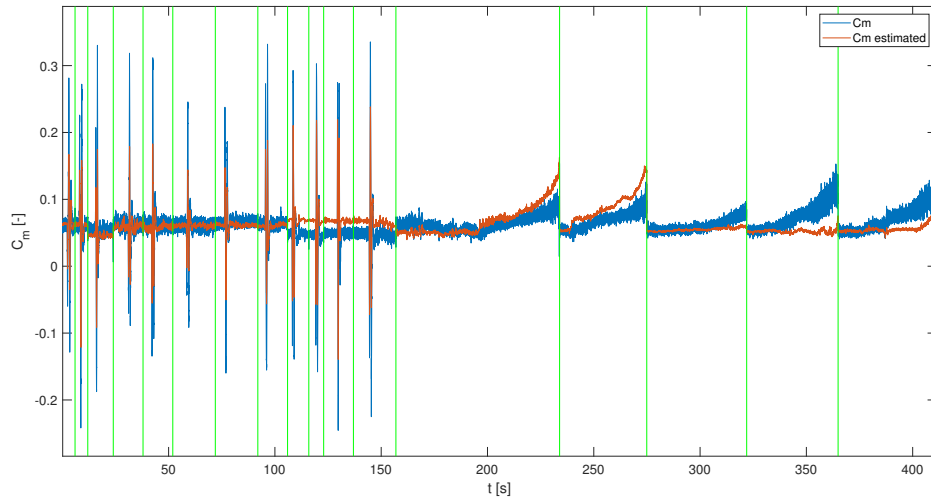


Figure 8.1: C_m regression with a base model

It was evident that, across some test points, there was an offset that was not covered by that model. These were the short period and stall manoeuvres with different configuration regarding the power setting and speed. For this purpose, thrust coefficient 7.7 was calculated, and its influence was introduced to the model by:

$$C_m = C_{m0} + C_{m\alpha}\alpha + C_{mq}q^* + C_{m\delta_e}\delta_e + C_{mC_T}C_T \quad (8.4)$$

This was proven to be quite an improvement to the model, as the fit of the estimated coefficient was matching to the calculated one better than before. In other words, the offset that was present in the older model was now greatly reduced. This can be seen, first on the figure 8.2, where closer view of only the short period manoeuvres is shown.

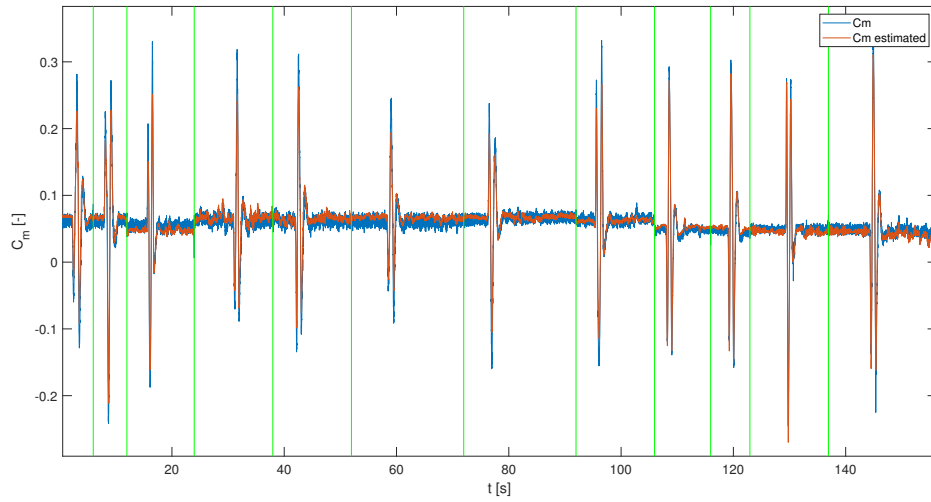


Figure 8.2: C_m regression with improved model, for a span of short period manoeuvres

Likewise, improvement of the fit can also be seen on figure 8.3, presenting the closer view of only the stall manoeuvres.

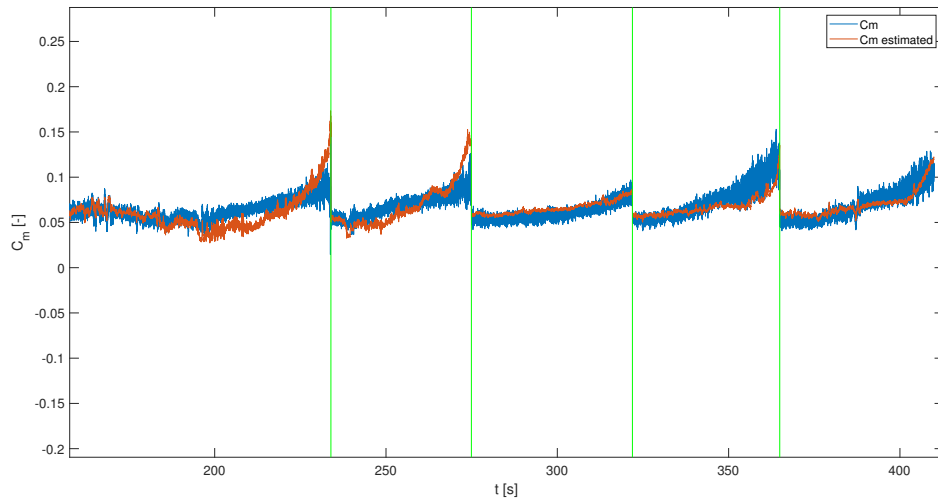


Figure 8.3: C_m regression with improved model, for a span of stall manoeuvres

Following the incorporation of the thrust coefficient as a parameter, manoeuvres per-

formed with different speed and power setting could also be covered by the model. Therefore, it was decided to keep that model and its parameters, shown in table 8.1.

Table 8.1: Estimated parameters for a pitching moment coefficient model

Parameter	Value
C_{m0}	0.093118
$C_{m\alpha}$	-0.014379
C_{mq^*}	-16.429
$C_{m\delta_e}$	-0.039408
C_{CT}	0.36746

It is important to mention that the relative error of each of the estimated parameters is less than 1% but with that being said, manoeuvres from flights with the identification number 6 and 11 were not incorporated in the estimation. With these manoeuvres, the estimation did not provide as good results so they were left aside not being covered by the model. This can be due to some inconsistencies during these flights, some unexpected atmospheric conditions or some other reasons. Also, it can be that another parameter and its influence, that is yet not incorporated, has to be included in the model. Anyway, that is left for further work analysis.

8.3.2. Lift force coefficient model

For the lift coefficient model development, as well for the drag coefficient model, phugoid and stall manoeuvres were chosen. Base model of the lift coefficient was not providing satisfactory results so it was at first improved introducing the effects of the pitch rate and the elevator deflection, like seen in [15]:

$$C_L = C_{L_0} + C_{L\alpha}\alpha + C_{Lq}q^* + C_{L\delta_e}\delta_e \quad (8.5)$$

This improved the regression significantly. Still, all manoeuvres from test flight 6 and phugoid manoeuvres from test flight 1 were not covered by the estimation. This led to the consideration of incorporating the thrust coefficient into the model, same like for the pitching moment coeff. model. Results of the estimation are shown on figures 8.4

and 8.5 for stall and phugoid manoeuvres respectively. Both figures come from the same estimation but are just representing a closer look of separate manoeuvres.

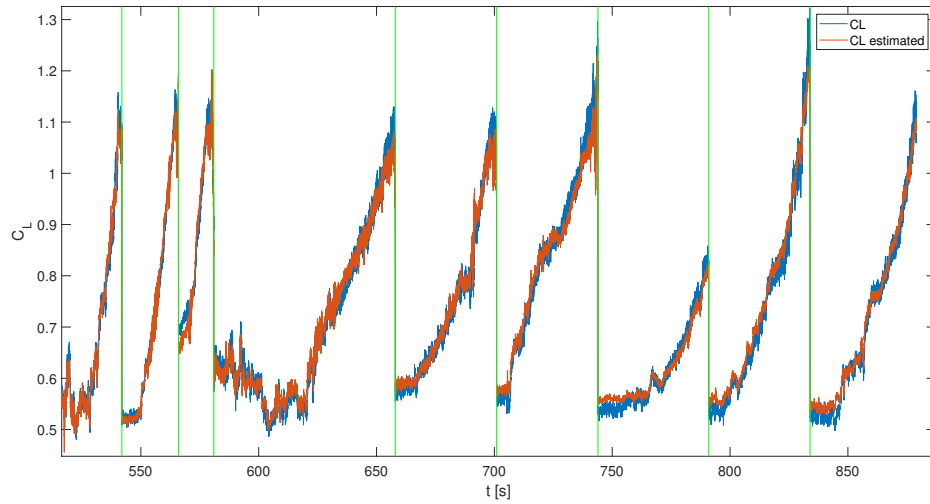


Figure 8.4: C_L model regression for a span of stall manoeuvres

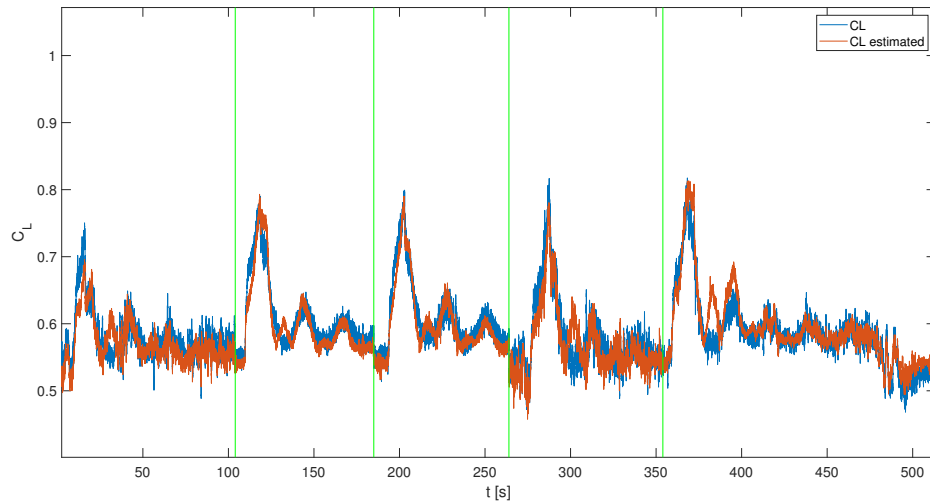


Figure 8.5: C_L model regression for a span of phugoid manoeuvres

These results, covering as well all the manoeuvres from flight 6, were proven to be

satisfactory so the model was set as valid:

$$C_L = C_{L_0} + C_{L\alpha}\alpha + C_{Lq}q^* + C_{L\delta_e}\delta_e + C_{LC_T}C_T \quad (8.6)$$

with the parameters shown in table 8.2.

Table 8.2: Estimated parameters for the lift force coefficient model

Parameter	Value
C_{L_0}	0.1608
$C_{L\alpha}$	0.050561
C_{Lq^*}	45.283
$C_{L\delta_e}$	0.0088616
C_{LC_T}	-0.09846

Like before, relative error of all estimated parameters is less than 1%.

8.3.3. Drag force coefficient model

In a similar manner, base model for the drag coefficient was also expanded with the influence of the thrust coefficient:

$$C_D = C_{D_0} + C_{D\alpha}\alpha + C_{DC_T}C_T \quad (8.7)$$

This model provided a satisfactory fit covering all the manoeuvres (stall and phugoid) from all the test flights. Influence of the quadratic value of the AoA $C_{D\alpha^2}\alpha^2$ was explored too but did not provide better results. That is why model was kept simple, not taking into account this parameter. Results of the estimation can be seen on figures 8.6 and 8.7 for stall and phugoid manoeuvres respectively.

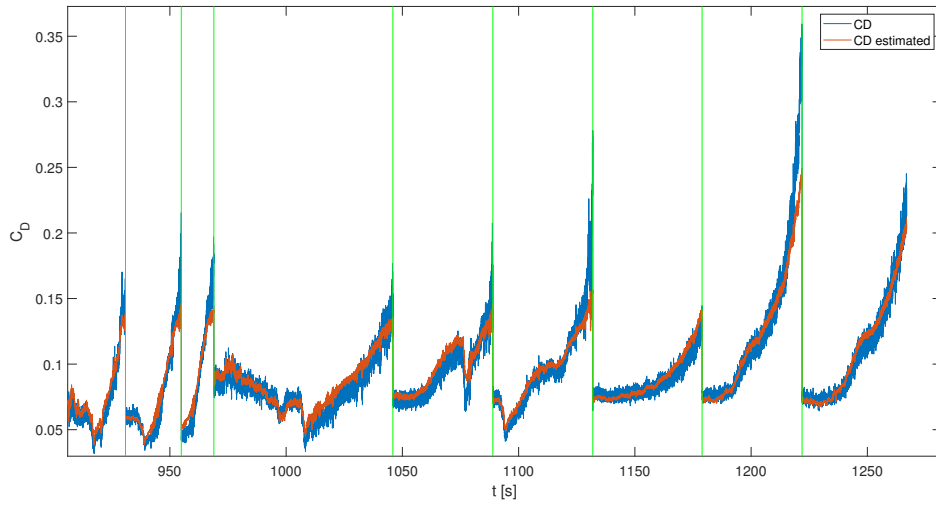


Figure 8.6: C_D model regression for a span of stall manoeuvres

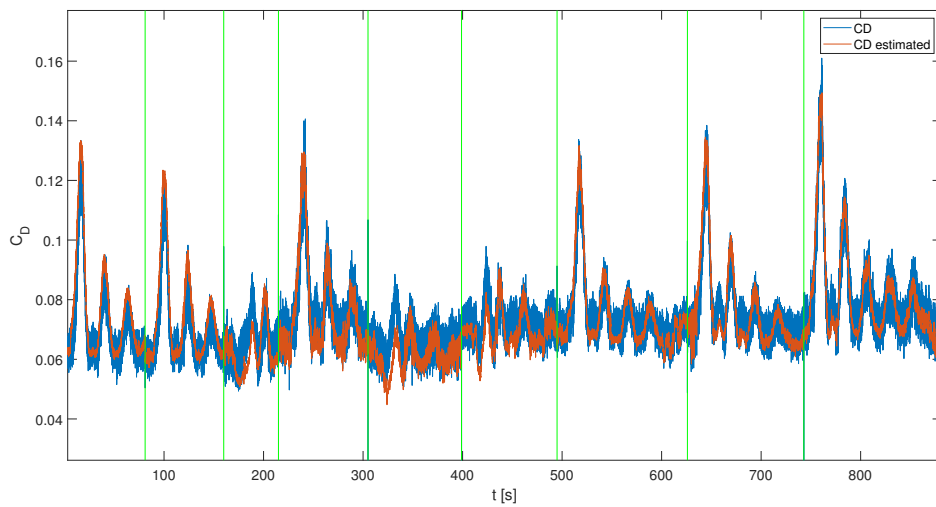


Figure 8.7: C_D model regression for a span of phugoid manoeuvres

Estimated parameters of the model are presented in table 8.3.

Table 8.3: Estimated parameters for the drag force coefficient model

Parameter	Value Base
C_{D0}	-0.018337
$C_{D\alpha}$	0.0081982
C_{DC_T}	0.3017

8.4. Lateral motion

Given limited time, lateral motion aerodynamic coefficient estimation was only briefly explored. For the side force coefficient C_Y model, only the steady heading steady sideslip manoeuvres were taken into account. For the roll C_l and yaw C_n moment coefficient models, only bank to bank and dutch roll manoeuvres were considered.

For C_Y , rudimentary, base model provided good enough fit covering all the manoeuvres (steady heading steady sideslip). Additionally, the influence of roll and yaw rate, as well as rudder deflection, was introduced [15]:

$$C_Y = C_{Y_0} + C_{Y\beta}\beta + C_{Yp}p^* + C_{Yr}r^* + C_{Y\delta_r}\delta_r \quad (8.8)$$

With so defined model, the results did not improve significantly. Since the premise is that the model should be as simple as possible, additional parameters were excluded and the model was reverted to the base one. Results given by the base model are shown on figure 8.8.

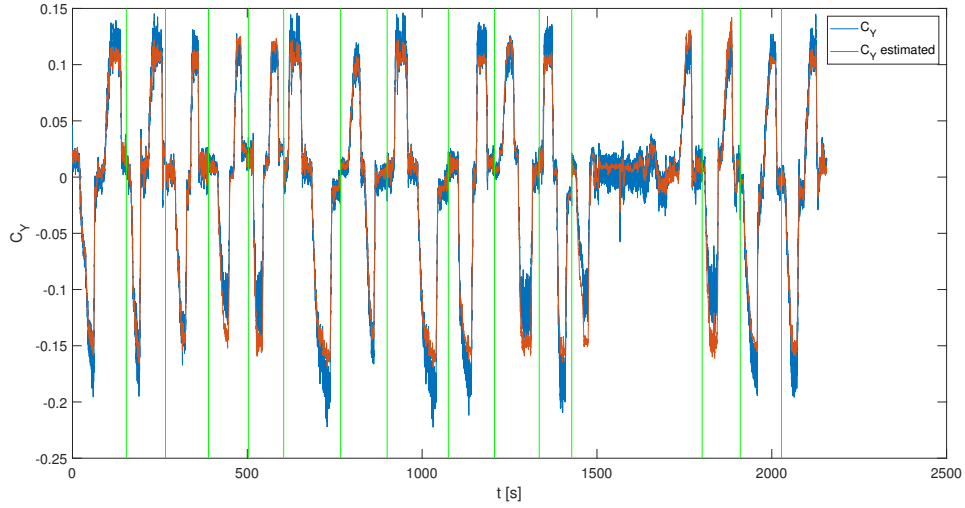


Figure 8.8: C_Y model regression for a span of steady heading steady sideslip manoeuvres

Estimated parameters are shown in table 8.4.

Table 8.4: Estimated parameters for the side force coefficient model

Parameter	Value Base
C_{Y0}	-0.0054128
$C_{Y\beta}$	-0.0066888

Roll and yaw moment coefficient base models were both expanded with rudder and aileron deflection parameters respectively [15]:

$$\begin{aligned}
 C_l &= C_{l0} + C_{l\beta}\beta + C_{lp}p^* + C_{lr}r^* + C_{l\delta_a}\delta_a + C_{l\delta_r}\delta_r \\
 C_n &= C_{n0} + C_{n\beta}\beta + C_{np}p^* + C_{nr}r^* + C_{n\delta_r}\delta_r + C_{n\delta_a}\delta_a
 \end{aligned}
 \tag{8.9}$$

Results of the regression for the yaw moment coefficient C_n model are presented on figure 8.9.

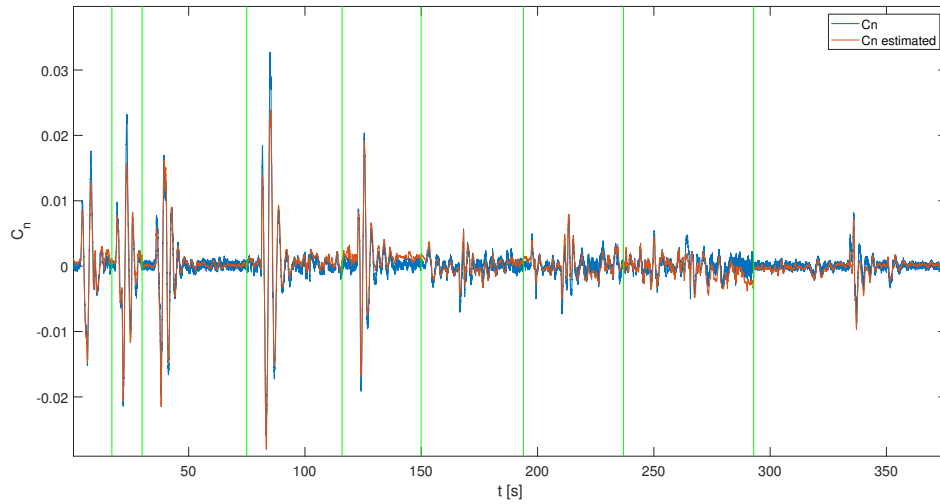


Figure 8.9: C_n model regression for a span of dutch roll and bank-to-bank manoeuvres

It is necessary to mention that manoeuvres from flight test under identification numbers 7 and 16 are not covered with this model. Estimated parameters of the model can be found in table 8.5.

Table 8.5: Estimated parameters for the yaw moment coefficient model

Parameter	Value
C_{n0}	0.0021345
$C_{n\beta}$	-0.0010037
C_{np^*}	0.12605
C_{nr^*}	0.077866
$C_{n\delta_r}$	0.00079484
$C_{n\delta_a}$	$6.8123 \cdot 10^{-5}$

Result of the regression for the roll moment coefficient model is not presented as the model was not enough researched. Still, the match is on the similar level as the one for the yaw moment coefficient model with the parameters shown in table 8.6.

Table 8.6: Estimated parameters for the roll moment coefficient model

Parameter	Value
C_{l_0}	0.0017471
C_{l_β}	0.00088847
$C_{l_p^*}$	0.34731
$C_{l_r^*}$	-0.10603
$C_{l_{\delta_r}}$	$-9.4282 \cdot 10^{-5}$
$C_{l_{\delta_a}}$	0.0018302

9 | Conclusions

Main goal of this thesis was the set up of the whole parameter estimation process with definition of some basic models for aerodynamic coefficients. Along the way, other necessary subsystems and methods have been advanced and revised. All is done with special care given to the transparency and repeatability for future students, working on the same project, to be able to follow and continue on the work. Work was carried out through following steps:

- Flight test data has been reprocessed in a more consistent way while the processing procedure is now documented and easily reproduced. As the final goal is data publishing, making it generally accessible, this was a precondition that had to be satisfied.
- Mass, balance and inertia estimation were all brought to a higher level of accuracy improving the calculations and adding the influence of more variables. CG position and moments of inertia of the aircraft are now all subjected to changes in aircraft configuration and mass.
- Even though the engine model itself was not directly and significantly improved, output provided by the model is matching to the measured parameters on more exact and consistent way.
- Flight test data was properly corrected and all the sensor error models have been improved reducing the errors to the data to the acceptable level.
- In the end, aerodynamic coefficients have been determined and all the parameters assembled for the estimation process. Linear regression is done and basic

exemplary models for the most of the coefficients have been offered.

It is left to incorporate all the developed subsystems into the existing PA-28 ReDSim model which could be the subject of the future work. Also, items of this work could be additionally improved and further researched. That being said, the mass, balance and inertia estimation could be brought to a higher level with the development of a more precise CAD model. Engine model could also be further developed what could provide exact outputs without the need of mapping the inputs. As well, sensor error models could be significantly enhanced covering more of the effects, not covered by the existing ones. Finally, parameter estimation, as it is just briefly explored, could further lead to much better and comprehensive models. Maybe with the use of more complex methods such as polynomials or Generalized Additive Models (GAM), as proposed in [4].

Bibliography

- [1] Kevin Spillman. Flight Testing of a General Aviation Aircraft and Simulation Model Development. Master's thesis, Zurich University of Applied Sciences, 2019.
- [2] Flavio Ferrari. Flight Testing of a General Aviation Aircraft and Aerodynamic Model Estimation. Master's thesis, Zurich University of Applied Sciences, 2019.
- [3] Ravindra V. Jategaonkar. *Flight Vehicle System Identification - A Time Domain Methodology*. Progress in Astronautics and Aeronautics, Volume 216. American Institute of Aeronautics and Astronautics, 2006.
- [4] M. Dettling R. Monstein, P. Capone and M. Vrdoljak. Determination of Model Structure from Flight Test with Generalized Additive Models. *JOURNAL OF AIRCRAFT*, 56(4), July-August 2019.
- [5] Vladislav Klein and Eugene A. Morelli. *Aircraft System Identification: Theory And Practice*. AIAA (American Institute of Aeronautics and Astronautics), 1st edition, 2006.
- [6] Airplane Maintenance Manual, Card 1 of 3, PA-28-151 CHEROKEE WARRIOR, PA-28-161 WARRIOR II, PA-28-161 WARRIOR III. 1995.
- [7] Warrior III PA-28-161 Pilot's Operating Handbook and FAA Approved Airplane Flight Manual. 2015.
- [8] Jan Roskam. *Airplane Design, Part V: Component Weight Estimation*. DARcorporation, 1985.

- [9] W. M. Gertsen R. L. Schmitt, K. C. Foreman and P.H. Johnson. *Weight Estimation Handbook for Light Aircraft*. 1959.
- [10] R. D. Finck. *USAF Stability and Control DATCOM*. 1978.
- [11] C. L. Best E. W Nelson and W. G. Mclean. *Schaum's Outline of Theory and Problems of Engineering Mechanics Statics and Dynamics*. McGraw-Hill, 5th edition, 1997.
- [12] S. Widnall J. Peraire. *Lecture L26-3D Rigid Body Dynamics: The Inertia Tensor*, Fall 2008.
- [13] Bernard Etkin. *Dynamics of atmospheric flight*. Wiley, 1972.
- [14] Jared A. Grauer. *Position corrections for airspeed and flow angle measurements on fixed-wing aircraft*. Technical report, 2017.
- [15] S. Janković. *Mehanika leta zrakoplova*. Sveučilište u Zagrebu FSB, 2002.

A | Appendix A

A.1. Flight Test Data Processing

A.1.1. Flight Test Data

- Folder: *Data Processing*
 - Folder: *Flight Test Data*
 - Folder: *Manoeuvre Data*
 - File: *Instructions for Data Processing by David Haber-Zelanto.docx*

A.1.2. Data Processing Utilities

- Folder: *Data Processing*
 - Folder: *Utilities*
 - File: *All_Data_processing.m*
 - File: *calibration.csv*
 - File: *cutToManoeuvres.m*
 - File: *Masterfile.xlsx*
 - File: *organizeData.m*
 - File: *procesData.m*
 - File: *signal_mapping_flight.xlsx*
 - File: *signal_mapping_manoeuvre.xlsx*

- File: *Single_flight_Data_processing.m*

A.1.3. Processed Data

- Folder: *Data*
 - Folder: *Flights*
 - Folder: *Manoeuvres*

B | Appendix B

B.1. Mass, Balance and Inertia Estimation

- Folder: *Utilities*
 - File: *getInertiaEsti.m*
 - File: *getInertiaEstiOEM.m*
 - File: *getMassEsti.m*
 - File: *getWnBData.m*
 - File: *PA28_estimation_mass_V1.m*
 - File: *PA28_mass_and_balance_V1.xlsx*

B.2. Propulsion

- Folder: *Utilities*
 - File: *getEngData.m*
 - File: *engine.slx*
 - File: *Init_Propulsion.m*

B.3. Flight Test Data Assembly and Corrections

- Folder: *Utilities*

- File: *getData.m*
- File: *getCorrSens.m*
- File: *getCGVel.m*
- File: *getAeroCeff.m*
- File: *lowPassFilter.m*

B.4. Modelling and Regression

- Folder: *Utilities*
 - File: *CD_estimation.m*
 - File: *Cl_estimation.m*
 - File: *CL_estimaton.m*
 - File: *Cm_estimation.m*
 - File: *Cn_estimation.m*
 - File: *CY_estimation.m*
 - File: *ols_fit.m*
 - File: *plotting.m*

B.5. Flight Path Reconstruction

- Folder: *FPR*

C | Appendix C

C.1. Measurements

During the visit to the hangar of the similar PA-28-161, some dimensions were measured and some coordinates of the IMU and the ADB were calculated.

C.1.1. IMU position

Coordinate x of the IMU, in ACS, was measured in [2] as $x = 3.3894$ m. Since the IMU is considered to be in the center of the airplane, y coordinate is $y = 0$ m. Coordinate z is measured (calculated) during the visit to the hangar, as a part of this thesis.

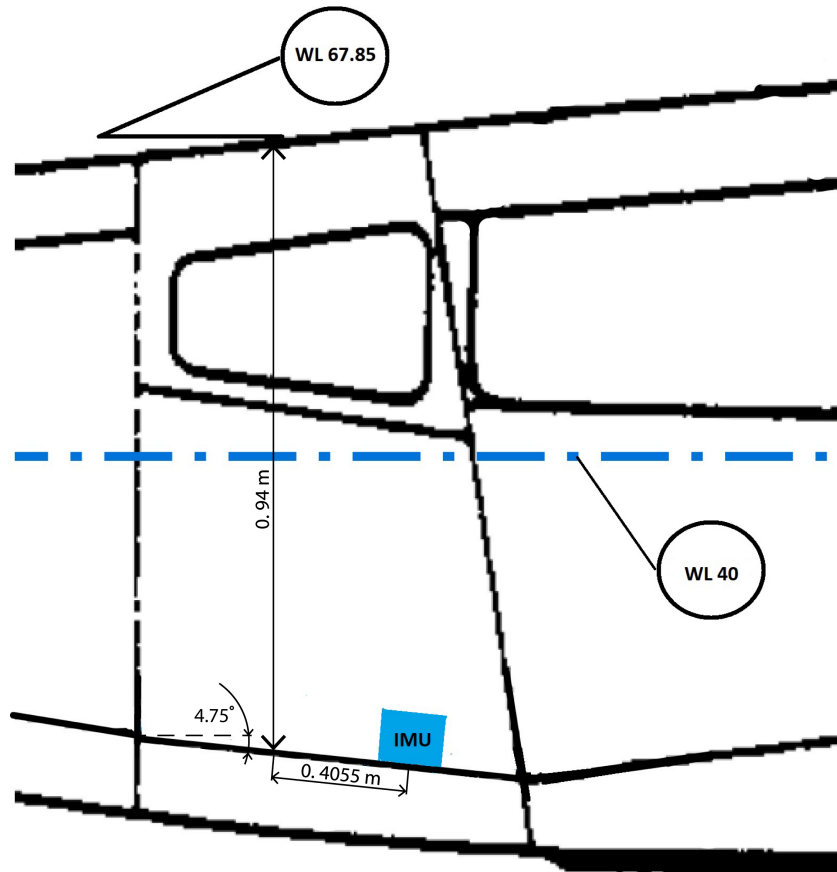


Figure C.1: Measuring IMU z position

It is calculated in a way:

$$z_{IMU} = -0.266 + 0.05 = -0.216 \text{ m}$$

where -0.266 m is calculated value from measures on figure C.1. Additional 5 cm is added because of the wooden board and half of the IMU height.

C.1.2. ADB position

ADB position was mostly defined in [2] and [1]. In ACS, z coordinate is $z = 0$ m since the ADB is aligned with the body frame x axis of the aircraft (fuselage centerline). From [2], y coordinate is $y = 5.31947$ m. Coordinate x was also defined in [2] but due to some inconsistencies, it was redefined here. Coordinate x is defined as:

$$x_{ADB} = (STA106.63 - 2.2)0.0245 - (l_{ADB} - 0.185) - l_{ex.rod} - 0.5 = 1.1735 \text{ m}$$

where $STA106.63 = 106.63$ in is the station reference in AMM (figure C.2) and 2.2 in is the offset of the coordinate system defined in POH (ACS) from the coordinate system defined in the AMM. 0.0245 is the conversion from inches to meters, $l_{ADB} = 0.42$ m is the length of the ADB [1], $l_{ex.rod} = 0.65$ m is the length of the extension rod from the wing leading edge to the start of the ADB [1]. 0.185 m is the distance from the beginning of the ADB (where it is connected to the rod) to the point between the two vanes (measured). 0.5 m (figure C.2) is the distance from the spar to the wing leading edge (measured).

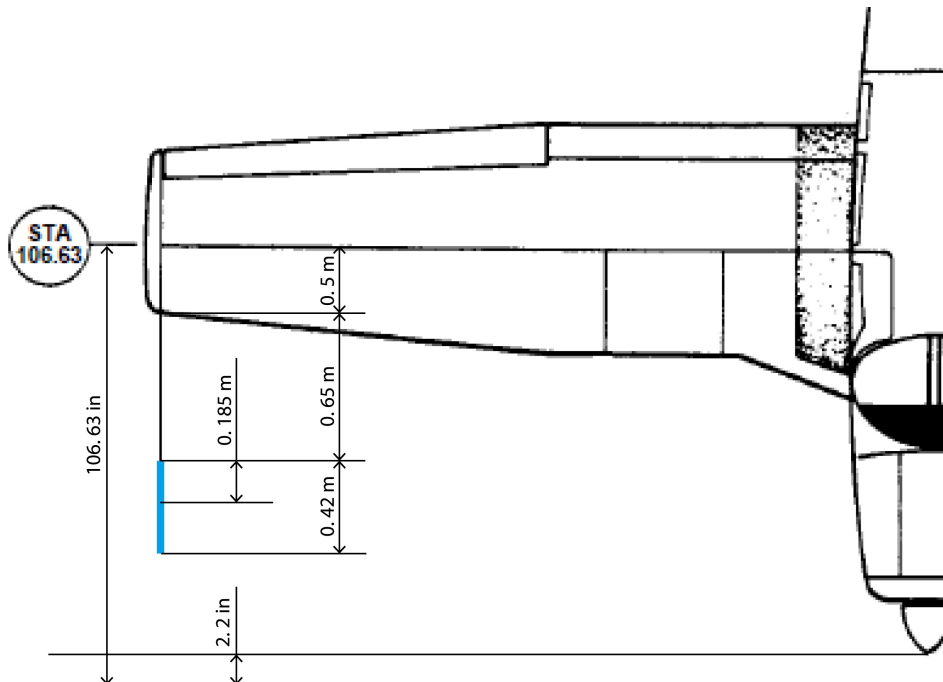


Figure C.2: Measuring ADB x position